

Discovery of PF-06873600, a CDK2/4/6 Inhibitor for the Treatment of Cancer

Kevin D. Freeman-Cook,* Robert L. Hoffman, Douglas C. Behenna, Britton Boras, Jordan Carelli, Wade Diehl, Rose Ann Ferre, You-Ai He, Andrea Hui, Buwen Huang, Nanni Huser, Rhys Jones, Susan E. Kephart, John Lapek, Michele McTigue, Nichol Miller, Brion W. Murray, Asako Nagata, Lisa Nguyen, Sherry Niessen, Sacha Ninkovic, Inish O'Doherty, Martha A. Ornelas, James Solowiej, Scott C. Sutton, Khanh Tran, Elaine Tseng, Ravi Visswanathan, Meirong Xu, Luke Zehnder, Qin Zhang, Cathy Zhang, and Stephen Dann



Cite This: *J. Med. Chem.* 2021, 64, 9056–9077



Read Online

ACCESS |



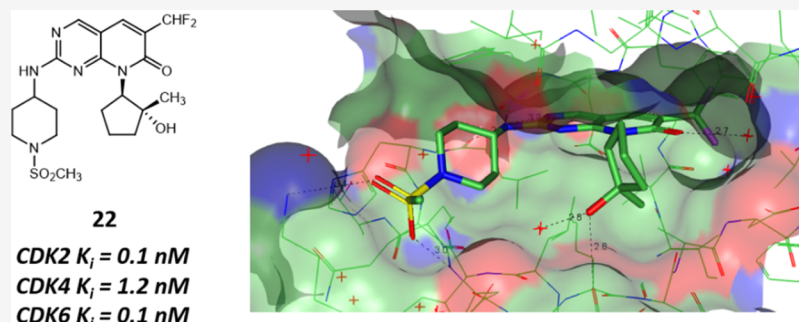
Metrics & More



Article Recommendations



Supporting Information



ABSTRACT: Control of the cell cycle through selective pharmacological inhibition of CDK4/6 has proven beneficial in the treatment of breast cancer. Extending this level of control to additional cell cycle CDK isoforms represents an opportunity to expand to additional tumor types and potentially provide benefits to patients that develop tumors resistant to selective CDK4/6 inhibitors. However, broad-spectrum CDK inhibitors have a long history of failure due to safety concerns. In this approach, we describe the use of structure-based drug design and Free–Wilson analysis to optimize a series of CDK2/4/6 inhibitors. Further, we detail the use of molecular dynamics simulations to provide insights into the basis for selectivity against CDK9. Based on overall potency, selectivity, and ADME profile, PF-06873600 (**22**) was identified as a candidate for the treatment of cancer and advanced to phase 1 clinical trials.

INTRODUCTION

The cyclin-dependent kinases (CDKs) are a 21-member family of serine–threonine kinases that are regulated by the formation of heterodimeric complexes with their cyclin-binding partners. CDK–cyclin complexes are involved in a diverse array of cellular processes, including transcriptional regulation (CDKs 7, 8, 9, 10, 11, 12, 13, 19, and 20), splicing (CDK 12), DNA repair (CDK 2, 9, and 12),¹ and regulation of the cell cycle (CDKs 1, 2, 4, and 6).² While each of the above could play an important role in the development of cancers, our research program focused on controlling the regulation of the cell cycle. The sequenced activation of the cell cycle CDKs orchestrates progression through each of the four distinct phases of the cell cycle (G1, S, G2, and M).³ First, CDK4 and CDK6 form complexes with cyclinD that phosphorylate the retinoblastoma (RB1) tumor suppressor. This step is followed by the CDK2–cyclinE complex performing additional phosphorylations on RB1.⁴ The entire process releases E2F transcription factors

from the RB1 complex and allows E2F-dependent transcription,⁵ permitting cells to move through the G1 phase and into the later phases of the cell cycle.

Sustained, unregulated progression through the cell cycle is a hallmark of cancer.⁶ The dysregulation of CDKs can cause continuous cell proliferation and can influence cancer progression and severity.⁷ Cyclin D amplification is a well-established oncogenic lesion, and targeting cyclin D activity with CDK4/6 inhibitors is a successful therapeutic strategy for treating some cancers.^{8,9} CDK2 has been proposed as a

Received: January 27, 2021

Published: June 10, 2021



therapeutic target in multiple tumor types such as KRAS-driven lung cancer,¹⁰ MYC-amplified neuroblastoma,¹¹ melanoma,¹² acute myeloid leukemia,¹³ hepatocellular carcinoma,¹⁴ glioblastoma,¹⁵ prostate cancer,¹⁶ and breast cancer.^{17–19} The cyclin-binding partners of CDK2 (cyclin E1 and cyclin E2) are amplified in a significant percentage of human cancers and this phenotype predicts poorer overall survival for patients.^{20,21}

The CDK4/6 dual inhibitor palbociclib (**1**, Figure 1) was approved in combination with letrozole in 2015 for the

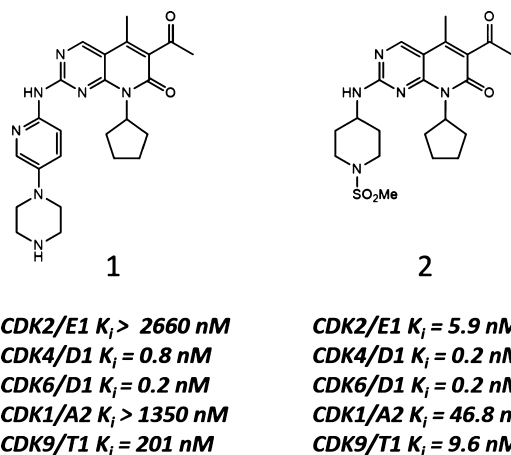


Figure 1. Palbociclib (**1**) and early file screening hit for CDK2/cyclinE1 (**2**).

treatment of estrogen receptor-positive (ER+) breast cancer. This was closely followed by two additional CDK4/6 inhibitors with roughly similar profiles, abemaciclib and ribociclib.²² While CDK4/6 inhibition in combination with endocrine therapy provides a therapeutic benefit in ER+ breast cancer, intrinsic and acquired resistance to CDK4/6 inhibition is expected. CDK2 activation may act as a compensatory mechanism for progressing through the cell cycle despite CDK4/6 inhibition. For instance, in the ER+ breast cancer cell line MCF7, siRNA knockdown of CDK2 alone appears to have very little effect on cell growth but synergizes with CDK4/6 inhibition.²³ More intriguingly, palbociclib-resistant MCF7 cells, generated through chronic palbociclib exposure, display relative amplification of cyclin E1, which has been shown to be oncogenic and indicative of high CDK2 activity.^{23,24} In this context, the siRNA knockdown of CDK2 or cyclin E1 re-sensitizes cells to palbociclib.²³ Indeed, a recent analysis of a palbociclib clinical trial revealed that patients with high cyclin E1 expression levels benefit less from palbociclib treatment than those with low cyclin E1 expression levels.²⁵ Therefore, adding inhibition of CDK2 to CDK4/6 could potentially help to control resistant tumors. Additionally, the broader control of CDK2, 4, and 6 could potentially benefit a wider scope of patients with tumors where CDK4/6 inhibitors have not yet been approved.

Work to develop CDK inhibitors has been ongoing for more than 20 years in the pharmaceutical industry. Flavopiridol, identified in 1992 from a plant source in India, was advanced into clinical trials in the late 1990s.^{26,27} Over the next two decades, academic and industrial researchers produced thousands of pre-clinical CDK inhibitors with widely varying activities, physical properties, and most importantly selectivity profiles. Generally, these compounds suffered from a lack of selectivity, both from within the CDK family and also from the

broader kinome.²⁸ When nonselective CDK inhibitors were dosed in clinical trials, they generally displayed cytotoxicity across gastrointestinal tissues, which could include irritation, nausea, diarrhea, and vomiting.²⁹ In addition, these compounds could cause pronounced cytotoxic effects on bone marrow cells, which resulted in the loss of peripheral leukocytes after 1–2 weeks of dosing.³⁰ Thus, while more than 20 CDK inhibitors started clinical trials over almost 30 years, to date only the selective CDK4/6 inhibitors (palbociclib, abemaciclib, and ribociclib) have been approved as cancer therapies. We hypothesized that much of the unwanted cytotoxicity in failed clinical candidates could arise from the inhibition of CDK1 because it had been shown to be essential in embryonic development in mice and because it has a central role in G2/M progression.³¹ Recognizing the overall challenge of designing selective chemical matter in a large kinase family, we embarked on a program attempting to develop compounds that would potently and selectively inhibit CDK2, as well as CDK4/6 while at the same time spare CDK1.

RESULTS AND DISCUSSION

Screening for biochemical CDK2 inhibition by mobility shift assay identified the truncated palbociclib derivative **2** (Figure 1). Compound **2** replaces the piperazine–pyridine ring system of the palbociclib structure with a methyl sulfonamide capped piperidine. This modification results in a greater than 500-fold increase in CDK2 potency compared to palbociclib but gives only modest CDK1 selectivity (8-fold). An examination of the crystal structure of compound **2** in complex with CDK2 is shown in Figure 2A and highlights the interactions leading to the dramatic increase in CDK2 activity. The piperidine sulfonamide motif made direct interactions with the CDK2 protein as a hydrogen bond acceptor from the backbone –NH of Asp86 and the sidechain –NH₃ of Lys89. Additionally, the piperidine ring was oriented within a lipophilic pocket with one edge forming van der Waals interactions with the phenyl sidechain of Phe82. Compound **2** was bound to CDK2 through a classical kinase hinge acceptor–donor–acceptor motif. Leu83 provided a carbonyl oxygen as an acceptor and a backbone NH as a donor, while Glu 81 presented a carbonyl oxygen as an acceptor. The methyl group at the 5-position of the pyridopyrimidinone ring system extended toward the gatekeeper Phe80 residue but primarily functioned to rotate the adjacent acetyl group out of the plane of the core bicyclic aromatic system. When oriented in this orthogonal conformation, the carbonyl oxygen served as a hydrogen bond acceptor for the backbone NH of Asp145. The lipophilic cyclopentyl ring was oriented within a lipophilic pocket formed by Val64, Leu134, and Ala144 with one edge that extended out toward a solvent accessible region.

The crystal structure of palbociclib (**1**) in complex with CDK6 is shown in Figure 2B. Many of the same interactions observed in the crystal structure of **2** in complex with CDK2 were present in the crystal structure of palbociclib in complex with CDK6. For example, the hydrophobic and hydrophilic interactions between the cyclopentyl ring, methyl ketone, and hinge interactions were similar in both protein–ligand complexes. Regarding primary sequence alignment, however, a single amino acid difference between these two protein–ligand complexes played a large role in driving significant differences in CDK2 potency and broader CDK isoform selectivity. While the hinge Phe residue is common to many CDK family members, including CDK1, 3, 5, 7, and 9, the

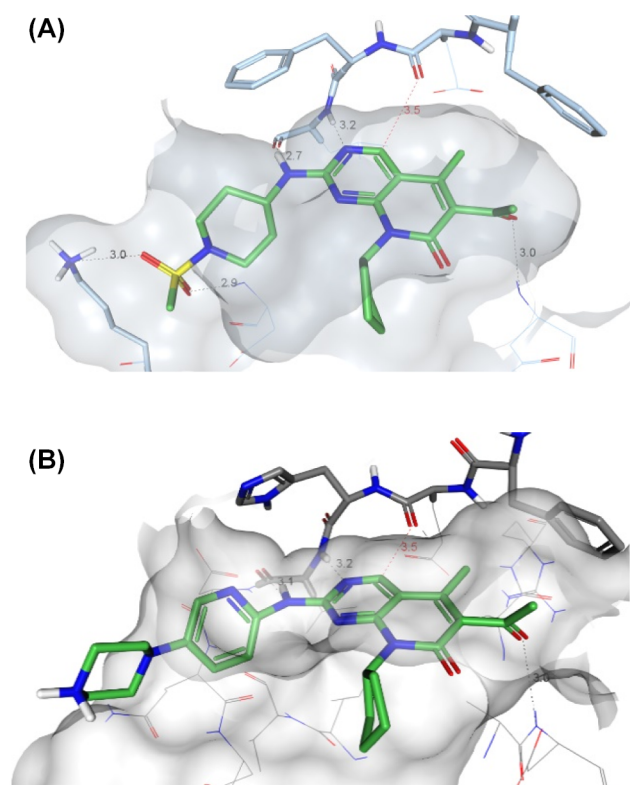


Figure 2. (A) Crystal structure of **2** in complex with CDK2. The protein surface is rendered in gray with key molecular interaction distances highlighted with dashed lines and measurements in Å. Sidechains of Phe80, Phe82, and Lys89 are bolded in the protein. The piperidine ring system orients a lipophilic edge toward Phe82. This group is similarly accommodated in other CDK isoforms as a relatively nonselective CDK inhibitor. (B) Crystal structure of palbociclib (**1**) in complex with CDK6. The protein surface is rendered in gray with key molecular interaction distances highlighted with dashed lines and measurements in Å. The His100 residue (bold) in CDK6 is aligned with the pyridyl nitrogen of palbociclib avoiding any de-solvation penalty between the protein and ligand.

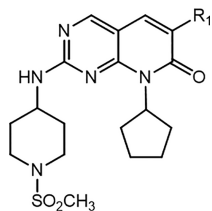
analogous residue in CDK4 is His95 and is His100 in CDK6. This key difference in the active site underpins the CDK isoform selectivity of palbociclib and the other marketed CDK4/6 dual inhibitors. Each of those molecules contains a pyridyl nitrogen atom which is placed in proximity to the histidine residue in the CDK4 and CDK6 complexes (shown for palbociclib in CDK6, **Figure 2B**). The polar environment around this His residue effectively solvated the pyridyl nitrogen in both CDK4 and CDK6 complexes, but the nonpolar Phe in other family members created a de-solvation penalty with the pyridine nitrogen on palbociclib and the other CDK4/6 inhibitors. This forms the basis of their extraordinary isoform selectivity. The aminopiperidine sulfonamide **2** (see **Figure 2A**) lacked the pyridyl nitrogen and oriented the hydrophobic edge of the piperidine ring toward the same Phe/His region. This change was tolerated by both an adjacent Phe or His residue, and thus **2** effectively inhibited multiple CDK/cyclin complexes (see **Figure 1**). The significant increase in CDK2 potency and modest level of CDK1 selectivity achieved with **2** provided an attractive starting point for designs to further increase CDK2 potency and CDK isoform selectivity.

A detailed examination of the crystal structure of **2** in complex with CDK2 suggested that the 5-methyl may have altered the position of the pyridopyrimidinone core within the

adenosine 5'-phosphate (ATP) binding pocket due to a potential close-contact with the gatekeeper Phe residue. Removal of both the 5-methyl and 6-acetyl groups from the pyridopyrimidinone core of **2** provided **3** (**Table 1**) which afforded a 7-fold improvement in CDK2 potency and a modest increase in CDK1 selectivity (16-fold). The CDK2 potency was further increased with compound **4** which was unsubstituted at the 5-position but incorporated a methyl at the 6-position. The addition of this methyl group resulted in 29-fold CDK1 selectivity, an improvement of 2-fold relative to the CDK1 selectivity of compound **3**. A crystal structure of compound **4** in complex with CDK2 (**Figure 3A**) revealed similar sulfonamide and hinge interactions observed with compound **2**. The 6-methyl was positioned at the opening of a pocket formed by Val64, Leu55, and Phe80, suggesting the opportunity to build additional interactions to increase CDK2 potency and potentially CDK isoform selectivity. Additionally, the cyclopentyl ring of compound **4** appeared to only partially fill a lipophilic pocket formed by Val64, Leu134, and Ala144.

A focus on lipophilic efficiency (LipE) informed the overall project objectives, medicinal chemistry analysis, and optimization strategy. As lipophilicity is a key parameter that influences metabolic stability, solubility, permeability, and overall safety risk,^{32–35} LipE was used to normalize potency differences relative to log *D*.³⁶ A comparison of compounds **3–5** which differ by only 6-position modifications (–H, –CH₃, and –Cl, respectively) demonstrated that all three analogues displayed relatively potent CDK2 *K_i* values. Compounds **4** and **5** are more lipophilic than compound **3**. Their additional lipophilicity was not used efficiently to improve their CDK2 binding potency relative to **3**. Consequently, the lipophilic efficiency suffered (LipE drops by 0.5 and 0.7 units, respectively, **Table 1**). Polarity was tolerated at the 6-position and analogues **6** and **7** gave LipE values which were essentially equivalent to parent analogue **3**. This argued that polar features could be accommodated without paying high de-solvation penalties and provided an opportunity to lower lipophilicity as a strategy to improve clearance and solubility. Hydroxyethyl analogue **8** possessed a similar LipE for CDK2 as **3** and one of the largest CDK2 versus CDK1 selectivity values (46-fold) observed in this series. The methyl ether analogue **9** also displayed similarly impressive CDK1 selectivity and suggested this selectivity was not dependent on the free hydroxyl group in **8**. However, the LipE drop of ~1 unit between compounds **8** and **9** suggested that the methyl group was not being used efficiently in binding to CDK2. The additional lipophilicity of **9** led to a large increase in HLM clearance. Repositioning of the oxygen atom within the ether chain of **9** to produce compound **10** caused a 40-fold reduction in CDK2 potency to 80 nM (*K_i*). Cyclopropyl derivative **11** recovered only a small amount of potency (35 nM, *K_i*) and compounds with larger 6-substituent groups such as **12** were completely inactive.

The impact on CDK1 selectivity with substitution at the 6-position of the pyridopyrimidinone core was noteworthy because CDK2 and CDK1 share a common Phe residue near this position. Despite this fact, installation of groups at the 6-position gave a small but generally consistent improvement in CDK1 selectivity. Compound **3** (6-hydrogen) displays a moderate 16-fold selectivity favoring CDK2 over CDK1 but, as noted earlier, replacement with the 6-methyl of **4** doubles this CDK isoform selectivity. This same improvement in CDK1 selectivity was seen in a series of 19 matched molecular pairs (MMPs) comparing a methyl versus hydrogen (**Figure**

Table 1. Modifications at the 6-Position (R_1) of the Pyridopyrimidinone Core^a

Compound #	R1	CDK2/cyclinE1 K_i (nM)	CDK4/cyclinD1 K_i (nM)	CDK6/cyclinD1 K_i (nM)	CDK1/cyclinA2 K_i (nM)	CDK9/cyclinT1 K_i (nM)	CDK1 / CDK2 (Fold Selectivity)	HLM Clint, app unbound (μ L/min/mg)	SFLogD at pH 7.4	LipE (CDK2 K_i)
3	H	0.71 \pm 0.02	0.67 \pm 0.21	0.88 \pm 0.17	11.7 \pm 0.9	41.3 \pm 3.0	16.5	81.5	2.4	6.7
4	Me	0.61 \pm 0.07	0.047 \pm 0.005	0.33 \pm 0.01	18.2 \pm 1.5	39.1 \pm 11.4	29.8	118	3.0	6.2
5	Cl	1.5 \pm 0.2	0.30 \pm 0.03	0.36 \pm 0.09	33.3 \pm 4.0	53.2 \pm 5.1	22.2	45.8	2.8	6.0
6		0.9 \pm 0.2	0.48 \pm 0.07	0.30 \pm 0.07	14.9 \pm 1.5	16.3 \pm 4.2	16.6	< 12.1	2.3	6.8
7		2.5 \pm 0.4	ND	0.19 (n=1)	29 (n=1)	15 (n=1)	11.6	12.4	1.9	6.7
8		1.6 \pm 0.2	0.48 \pm 0.06	0.92 \pm 0.24	74.4 \pm 9.9	132 \pm 43	46.5	< 23.9	2.2	6.6
9		2.17 \pm 0.06	0.196 \pm 0.003	1.73 \pm 0.78	115.6 \pm 15.3	163 \pm 39	53.3	272	2.9	5.8
10		82.4 \pm 10.8	0.21 \pm 0.01	1.78 \pm 0.21	534 \pm 68	> 1200 (n=3)	6.5	< 37.9	3.1	4.0
11		38.1 \pm 9.8	0.10 \pm 0.02	1.44 \pm 0.19	536 \pm 122	> 1400 (n=4)	14.1	126	3.3	4.1
12		1360 (n=1)	ND	0.86 (n=1)	> 1350 (n=1)	> 1200 (n=1)	ND	< 13.6	3.3	2.6

^a K_i values are the arithmetic mean of at least three independent replicates \pm SEM, except where noted. Each individual K_i value is generated from at least 10 single-point inhibition data points run in duplicate. LipE values are calculated using the CDK2 K_i value, according to the formula LipE = $pK_i - \log D$.

3B). An examination of the overall trend within these MMPs highlighted an average 2.3-fold improvement in CDK1 selectivity (CDK1 K_i /CDK2 K_i) when comparing hydrogen versus methyl in this position (Figure 3C), and in some instances this isoform selectivity improvement reached over 6-fold. These results suggested that CDK1 was generally less tolerant of steric bulk in this region. This is despite the fact that the Phe gatekeeper residue is the same in both CDK1 and CDK2, and the 3-dimensional surface that surrounds compound 4 is also quite similar between CDK1 and CDK2 (see Figure 3D). This surprising difference in potency between the two isoforms may be a result of very small differences in protein strain energy between CDK1 and CDK2, which are difficult to accurately predict.

Because compound 8 displayed one of the highest levels of CDK1 selectivity, it was selected as a tool compound to evaluate the potential for the translation of biochemical activity and selectivity into cellular systems. Both Kuramochi and OVCAR3 ovarian cancer cell lines were selected as model systems due to their similar dependence on CDK2 as a primary oncogenic driver. In these cell lines, compound 8 inhibited the phosphorylation of RB1 while selective CDK4/6 inhibitors such as palbociclib (1) were unable to do so (see Figure 4A). The inhibition of the phosphorylation of RB1 led to the inhibition of proliferation (see Figure 4B) and produced a strong G1 arrest, with a significant reduction of the population of cells in the S-phase (see Figure 4C). Palbociclib was inactive in each of these experiments with CDK2-driven cell lines but did show analogous activity in similar experiments using CDK4-driven ER+ breast cancer cell lines.²³ Live cell target engagements for both CDK2 and CDK1 were measured in

order to evaluate how the biochemical selectivity ratios translated into the cell context (see Figure 4D). Kuramochi cells were pre-incubated with compound 8, followed by treatment with the broad-spectrum covalent kinase probe XO44 (PF-6808472),³⁷ then lysed and subjected to a copper catalyzed azide-alkyne cycloaddition reaction with biotin-linked azide. After enrichment with streptavidin beads, elution, and SDS-PAGE, western blots could quantitate the occupancy of 8 on different CDK isoforms. In line with biochemical K_i measurements, pre-incubation of 8 efficiently prevented the binding of XO44 to CDK2. As a less potent inhibitor of CDK1, compound 8 was much less effective in blocking XO44 binding to CDK1. From these experiments, a concentration to give 50% kinase occupancy (OC_{50}) for 8 in the cells was calculated for each isoform. The OC_{50} values for CDK2 of 200 nM and 4 μ M for CDK1 (20-fold ratio) were consistent with the CDK2 pRB1 cellular inhibition IC_{50} (270 nM), the cellular growth inhibition IC_{50} (240 nM), and the biochemical CDK1/CDK2 K_i ratio of 46-fold.

To rapidly evaluate potential opportunities that the vector for the 8-position provided for increasing CDK2 potency and isoform selectivity, a combination of the structure-based drug design and Free-Wilson analysis was used. As noted in the crystal structure of 2 in complex with CDK2, the hydrophobic pocket formed by Val64, Leu134, and Ala144 suggested that increasing lipophilicity in this region of the protein could provide increases to CDK2 potency. Steric interactions would predispose cyclic structures to orient orthogonally to the plane of the pyridopyrimidinone core, and it appeared that this orientation would provide additional positions for further substituents to optimize binding to CDK2. Computational

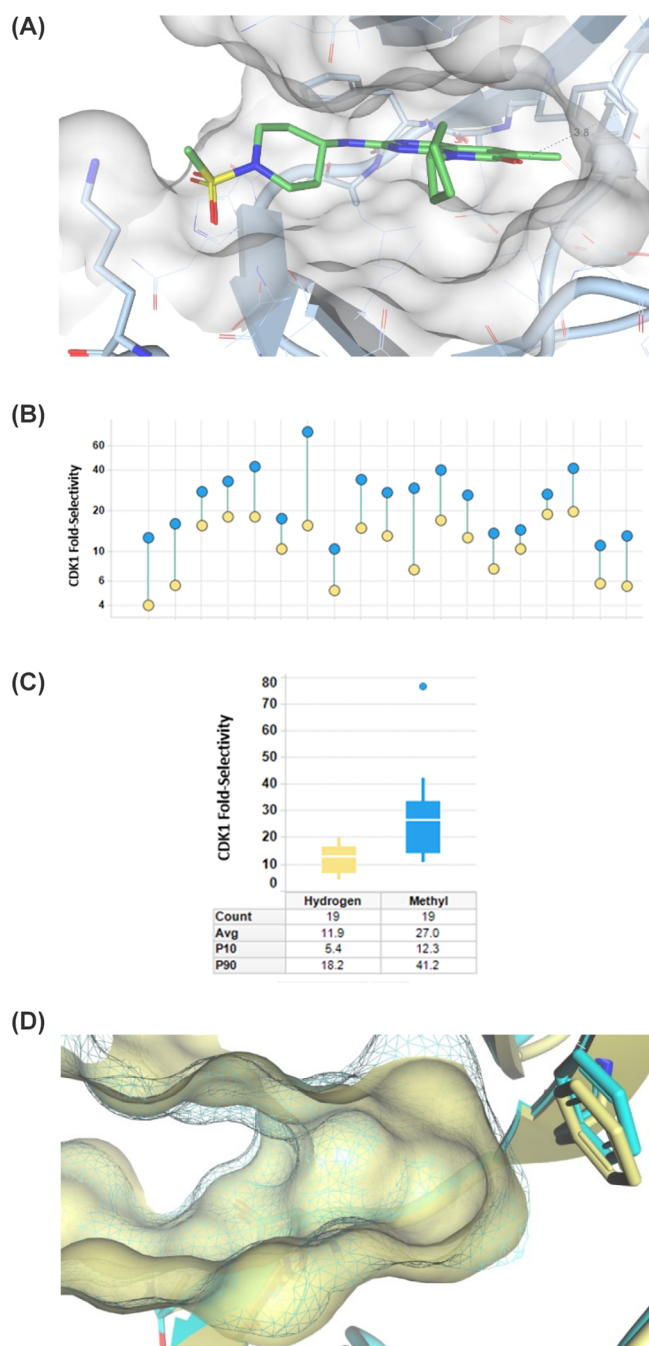


Figure 3. (A) Crystal structure of **4** in complex with CDK2. The protein surface is rendered in gray. Lys89, Phe82, and Phe80 are bolded in the protein. The 6-position methyl is oriented towards a pocket formed by the sidechains from the C- α -helix and the gatekeeper Phe80. (B) Matched pairs of compounds which differ only by the presence of a methyl group (blue circles) or hydrogen atom (yellow circles) and the effect on biochemical selectivity vs CDK1 (ratio of biochemical K_i CDK1/biochemical K_i CDK2). (C) Box and whisker plot of pairwise data from (B). (D) Surface representations of CDK2 (wireframe, teal) and CDK1 (solid, yellow) around the inhibitor binding pocket formed by **4**. Phenylalanine gatekeeper residues are also highlighted for CDK2 (teal) and CDK1 (yellow).

deconstruction of pyridopyrimidinone analogues from the Pfizer compound collection using a Free–Wilson technique³⁸ gave further insights into features that would provide both high potency and high LipE.³⁹ In this analysis, 151 variations in R_3

(see Figure 5A) and 92 different substituent variations from the combination of R_1/R_2 from a total of 324 analogues were analyzed to determine their mathematical contribution to potency and lipophilic efficiency. To assess this analysis, all the historical analogues were subjected to a leave-one-out (LOO) validation method, which produced an R^2 value of 0.74 for the 148 resulting analogues (Figure 5B). This LOO technique suggested a high degree of consistent binding in the historical data set and the potential for good predictivity of new combinations. Potential groups in both vectors were then ranked and prioritized for synthesis.

Combining the observations from the structural analysis of inhibitor CDK2 complexes with the Free–Wilson methodology, designs were selected for synthesis. Considerations included the potential for delivering analogues with high potency as well as a focus on balancing lipophilicity to provide the potential for low human liver microsomal clearance (HLM Cl_{int} , Table 2). In the R_3 vector, no groups provided any predicted improvement from the established amino-piperidine sulfonamide motif. While some variations were attempted, efforts to improve the potency of compounds by modifications in this region were generally unsuccessful and, in many cases, only increased synthetic complexity. On the other hand, in the vector formed from R_1/R_2 , the Free–Wilson methodology provided many possible alternatives to improve potency and LipE. These modifications became the focus of further optimization efforts. Swapping cyclopentyl (**3**) with cycloheptyl (**13**, Table 2) improved CDK2 potency and maintained a similar LipE. The increased HLM clearance observed for **13** was a consequence of increased lipophilicity compared with **3**. Cyclohexyl derivative **14** showed a significant drop in LipE as the CDK2 potency was reduced while lipophilicity increased. The addition of a methyl group to the cyclopentyl ring formed the (1*R*,2*S*)-2-methylcyclopentyl derivative **15**. This analogue oriented the methyl group to occupy the bottom of the lipophilic pocket in CDK2 formed by Ala144, Leu134, and Val64. This became a key design feature. Both CDK2 potency (0.09 nM K_i) and CDK1 selectivity (26-fold) were improved. Not unexpectedly, the increase in lipophilicity that accompanied the additional methyl group substituent in **15** led to an increased turnover in human liver microsomes. Some of the higher clearance was alleviated in isobutyl analogues **16** and **17** which had lower SFlogD values (*ca.* 2.2). Although these derivatives had all the atoms necessary to reach into the same lipophilic pocket as **15**, the more polar acyclic structures provided less binding efficiency and lower CDK1 selectivity. This may be due to small amounts of strain required in these acyclic systems to optimally reach the pocket. Another possibility is that cyclic structures such as **15** not only benefited from the lipophilic pocket interactions as described but also van der Waals interactions between ring carbons and residues Gly11 and Val18 that form the G-loop which sits adjacent to the inhibitor. These interactions from ring carbons would be missing in acyclic systems. Finally, the data for isopropyl derivative **18** suggested that while low HLM clearance was possible with much lower SFlogD, potency suffered as the occupation of the lipophilic pocket was not possible.

The group which was identified from the Free–Wilson analysis as providing the overall highest contribution to LipE was the (1*R*,2*R*)-2-hydroxy-2-methylcyclopentyl moiety. Computational modeling and analysis of the separate roles of the methyl and hydroxyl groups revealed important details of the

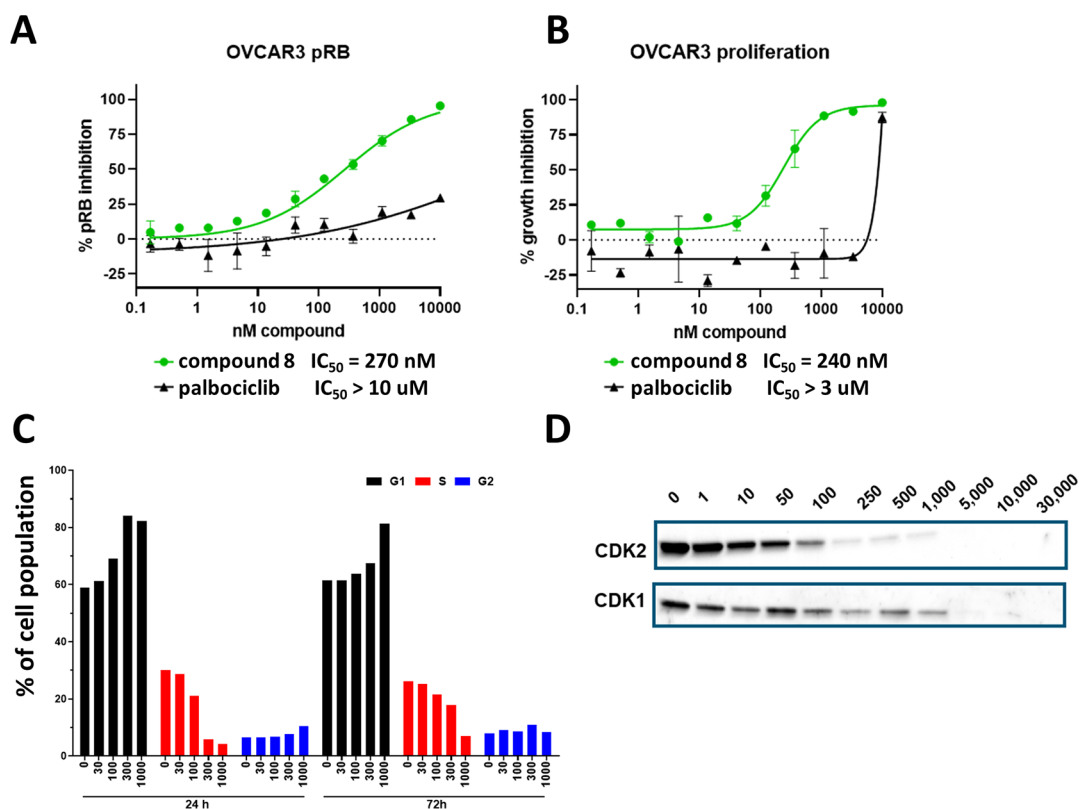


Figure 4. (A) Inhibition of the phosphorylation of RB1 in OVCAR3 cells for both palbociclib and 8. (B) Inhibition of proliferation in OVCAR3 cells for both palbociclib and 8. (C) BRDU cell cycle analysis of cell cycle arrest in OVCAR3 cells for 8 at 24 and 72 h. Compound concentration (nM) is shown below each bar, and the proportion of cells in G1 (black), S (red), and G2/M (blue) are shown. (D) Western blot of compound 8 showing the differential blocking of XO44 binding in CDK2 and CDK1 in Kuramochi cells demonstrating differential cellular target engagement. Compound concentration (nM) is shown above each lane of the blot.

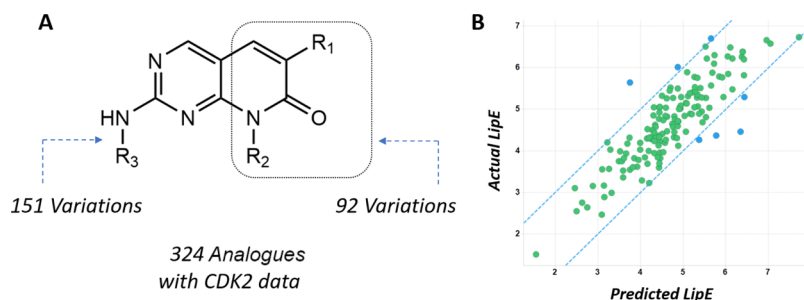
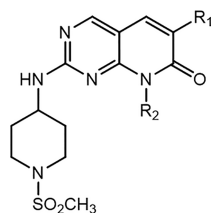


Figure 5. (A) Free-Wilson schematic. 324 Pyridopyrimidinone analogues were computationally deconstructed to form hypothetical fragments and determine each fragment's contribution to LipE. (B) Leave-one out analysis of 148 analogues. Blue circles designate compounds which differed in actual vs. predicted LipE by more than 1 unit. 141/148 (95%) of analogues (green circles) differed by less than 1 LipE unit.

likely binding mode. The methyl group appeared to fill the lipophilic pocket in CDK2 in a manner as described above for compound 15. The modeling also showed that the hydroxyl group could be positioned to form a hydrogen bond with a backbone carbonyl from Gln131, and importantly, it reduced the calculated SFlogD by \sim 1 unit. Compound 19 which contains the (1*R*,2*R*)-2-hydroxy-2-methylcyclopentyl substituent was a breakthrough compound with impressive CDK2 potency (0.2 nM), LipE (8.2), and the potential for optimization for further improvements in selectivity and HLM Cl_{int} . An additional feature of lead compound 19 was the high level of CDK9 selectivity. The presence of the piperidine sulfonamide group pre-disposed our compounds toward a high level of selectivity against CDK9 (see Figure 6A). Additionally, the installation of the (1*R*,2*R*)-2-hydroxy-2-

methylcyclopentyl group appeared to enhance that selectivity. To investigate this improved CDK9 selectivity, we employed molecular dynamics (MD) simulations to compare ligand–protein dynamics for compound 19 in both CDK2 and CDK9 (see Figure 6B).

The MD simulation with CDK2 suggested that the sulfonamide formed a hydrogen bond interaction with the backbone NH of Asp86, which was shielded from bulk water molecules by a large hydrophobic sidechain (Lys89). This hydrogen bond caused the sulfonamide region to remain stable and tightly bind to CDK2 throughout the course of the simulation. That tight binding influenced similar tight binding in the adjacent lipophilic pocket where the tertiary hydroxyl and the methyl group from the cyclopentyl ring formed favorable interactions with CDK2. Specifically, the hydroxyl

Table 2. Modifications at the 6-Position (R_1) and 8-Position (R_2) of the Pyridopyrimidinone Core^a

Compound #	R1	R2	CDK2/cyclinE1 K_i (nM)	CDK4/cyclinD1 K_i (nM)	CDK6/cyclinD1 K_i (nM)	CDK1/cyclinA2 K_i (nM)	CDK9/cyclinT1 K_i (nM)	CDK1 / CDK2 (Fold Selectivity)	HLM Clint, app unbound (μ L/min/mg)	SFLogD at pH 7.4	LipE (CDK2 K_i)
13	H	cycloheptyl	0.36 ± 0.05	0.56 ± 0.13	1.17 ± 0.08	6.7 ± 0.4	8.0 ± 1.7	18.6	367	3.0	6.5
14	H	cyclohexyl	2.6 ± 0.5	0.52 ± 0.11	1.29 ± 0.77	31.4 ± 11.7	6.2 ± 2.0	12.1	139	2.8	5.8
15	H		0.09 ± 0.01	0.80 ± 0.12	1.15 ± 0.06	2.4 ± 0.6	21.4 ± 3.4	26.7	> 482	3.0	7.1
16	H		1.61 ± 0.05	1.66 ± 0.28	2.02 ± 0.93	8.8 ± 1.7	18.4 ± 5.2	5.5	122	2.1	6.7
17	H		0.88 ± 0.06	1.57 ± 0.11	1.16 ± 0.10	4.8 ± 0.2	22.7 ± 1.8	5.5	132	2.2	6.8
18	H		4.3 ± 0.1	8.33 ± 0.68	6.60 ± 0.28	35.6 ± 1.2	109.0 ± 4.2	8.3	14.1	1.9	6.5
19	H		0.20 ± 0.01	2.19 ± 0.07	1.07 ± 0.08	4.4 ± 0.3	30.0 ± 1.8	22.0	36.4	1.5	8.2
20	Cl		0.20 ± 0.02	0.45 ± 0.28	0.37 ± 0.12	7.3 ± 0.8	36.8 ± 1.7	36.5	< 13.7	1.8	7.9
21	Me		0.12 ± 0.03	1.08 ± 0.09	0.24 ± 0.01	5.5 ± 0.8	31.4 ± 3.0	45.8	67.4	2.0	7.9
22	CHF ₂		0.13 ± 0.01	1.25 ± 0.08	0.11 ± 0.01	4.5 ± 0.4	19.6 ± 1.6	34.6	< 10.8	1.9	8.0
23	CH ₂ CH ₂		0.11 ± 0.01	0.19 ± 0.02	0.064 ± 0.003	2.9 ± 0.3	8.0 ± 0.9	26.4	19.1	2.2	7.8

^a K_i values are the arithmetic mean of at least three independent replicates ± SEM. Each individual K_i value is generated from at least 10 single-point inhibition data points run in duplicate. LipE values are calculated using the CDK2 K_i value, according to the formula LipE = $pK_i - \log D$.

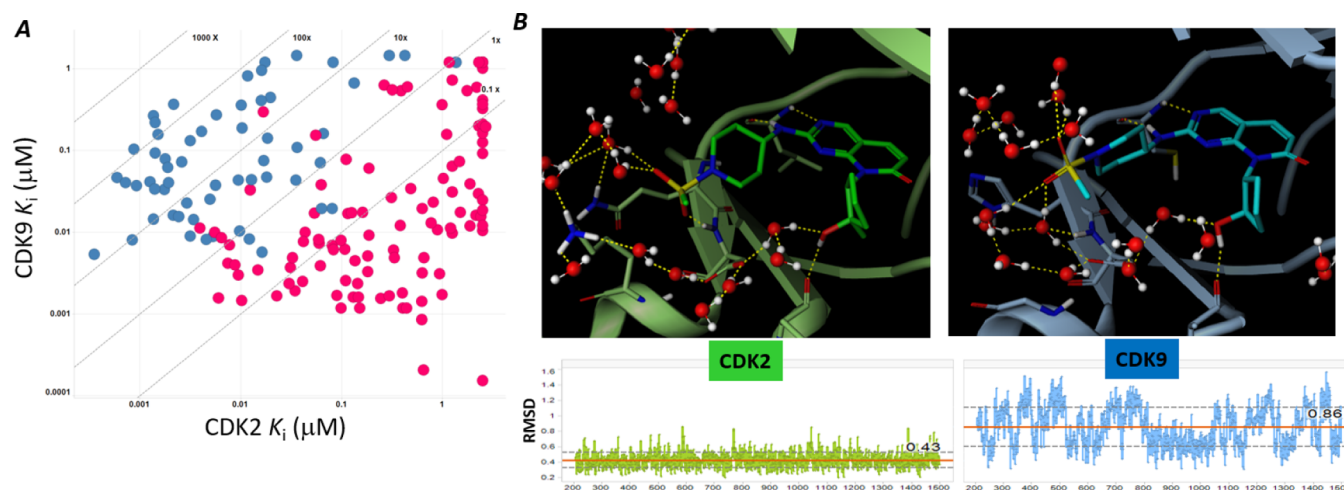


Figure 6. (A) Scatter plot of CDK2 vs CDK9 potency (K_i in μ M). Lines of equal selectivity are plotted as diagonals, with selectivity increasing to the top left of the plot. Compounds containing the piperidine sulfonamide motif are plotted as blue dots, all other compounds are plotted as red dots. (B) Snapshots from MD simulation of compound 19 in CDK2 (top left) and CDK9 (top right). Root-mean-squared deviation (rmsd) plots showing movement over the course of the entire simulation are plotted below each snapshot vs time in picoseconds (CDK2 in green and CDK9 in blue).

formed a hydrogen bond with a backbone carbonyl of Gln131 while the methyl group occupied the lipophilic pocket

previously described. Together, this entire set of interactions caused compound 19 to remain tightly associated with the

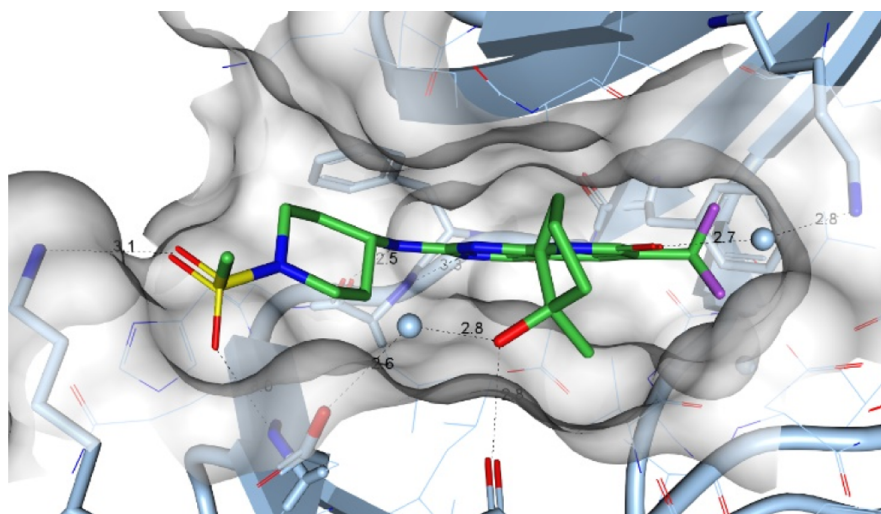


Figure 7. Crystal structure of **22** in complex with CDK2. The protein surface is rendered in gray with key molecular interaction distances highlighted with dashed lines and measurements in Å. Lys89, Asp86, Phe82, Phe80, and Gln131 are bolded in the protein. The methyl group on the cyclopentyl ring is positioned in a lipophilic pocket formed by residues Val64, Leu134, and Ala144.

CDK2 protein. In contrast, CDK9 lacks Lys89 and the corresponding residue is Gly112 which creates a much more open pocket. This additional space allowed bulk water to more easily solvate the backbone NH of Asp109. Without the oxygen atom of the sulfonamide being fully engaged in a direct hydrogen bonding interaction, the sulfonamide moiety fluctuated in position throughout the simulation. Occasionally, this movement resulted in direct hydrogen bonding between the inhibitor's sulfonamide and the backbone NH of Asp109, but more often the sulfonamide group moved away and allowed a bulk water molecule to solvate this NH. This fluctuation resulted in the movement of the core of the inhibitor itself and caused the tertiary hydroxyl to interact less effectively with the backbone carbonyl. The net result of the inhibitor fluctuation in the CDK9 protein was that both ligand and protein experienced partial de-solvation penalties and thus reduced binding affinity. Additionally, primary sequence differences between CDK9 and CDK2 around the backbone carbonyl account for increased flexibility. The sequence in CDK9 is Ala152-Ala153, while in CDK2 the corresponding residues are Pro130-Gln131. These differences appear to have accentuated the increased movement observed in the CDK9 protein and correspondingly led to weaker CDK9 binding through the hydrogen bond to the tertiary hydroxyl group of **19**. The differences in movement throughout the simulation are shown in the CDK2 (green) and CDK9 (blue) rmsd plots in Figure 6B. While the MD simulation was only a calculation of potential protein–ligand interactions, it appeared to highlight the structural features in both the ligand as well as the two proteins which help explain the observed tight binding of **19** to CDK2 and weaker binding to CDK9.

Compound **19** possessed many of the characteristics which were desired in a final clinical candidate but poor microsomal stability led to a predicted short human half-life inconsistent with once or twice daily dosing. The examination of the site of metabolism in **19** revealed a propensity for metabolic oxidation occurring at the 6-position of the pyridopyrimidinone core. New derivatives were designed to reduce or block oxidative metabolism at that position. As discussed earlier for 6-substituents, this strategy could additionally provide the added benefit of a slight ($\sim 2\times$) improvement to the CDK1

selectivity. Synthesis of the 6-chloro substituent gave **20**, an analogue with improved HLM clearance and favorable CDK1 selectivity. The methyl derivative **21** possessed improved CDK1 selectivity but significantly increased the human microsomal clearance. Analysis of the site of metabolism for **21** indicated that significant p450 mediated oxidation occurred on the 6-methyl substituent. Difluoromethyl analogue **22** (PF-06873600) was designed to maintain favorable CDK1 selectivity and to specifically address HLM clearance liability. Replacing the 6-methyl with the $-\text{CHF}_2$ substituent reduced the oxidative metabolic liability and gave an analogue with significantly improved microsomal clearance and still high CDK1 selectivity ($\sim 34\times$). One consideration with **22** was a lower CDK4/D1 potency than for some other analogues and as a result, a low selectivity ratio between CDK4/D1 and CDK1/A2. Di-fluoroethyl derivative **23** was a similarly noteworthy design with improved CDK4 potency compared to compound **22**, albeit with higher HLM Cl_{int} which makes the overall profile of **23** less attractive.

A crystal structure of compound **22** in complex with CDK2/cyclinE (Figure 7) highlighted several of the key interactions which were very similar to those described for compound **4**. The 4-aminopiperidine sulfonamide moiety provided lipophilic and polar interactions with the CDK2 protein. The piperidine ring was oriented within a lipophilic pocket with one edge forming van der Waals interactions with the sidechain phenyl of Phe82. One of the oxygen atoms from the sulfonamide group served as a hydrogen bond acceptor for the backbone $-\text{NH}$ of Asp86, while the other oxygen was engaged in a hydrogen bond with the sidechain $-\text{NH}_3$ of Lys89. The 4-amino $-\text{NH}$ of the piperidine ring along with the 3-position nitrogen and 4-hydrogen of the pyridopyrimidinone core provided the canonical hinge hydrogen bonds with the NH and carbonyl of Leu83 and backbone carbonyl of Glu81. As expected, the (1*R*,2*R*)-2-hydroxy-2-methylcyclopentyl ring system filled a lipophilic pocket formed at the top by the G-loop residues Gly11 and Val18 and at the bottom by Val64, Leu134, and Ala144. The methyl substituent appeared to optimally fill this bottom lipophilic pocket, while the hydroxyl group was positioned to form a hydrogen bond with the backbone carbonyl of Gln131 and a water molecule. Finally,

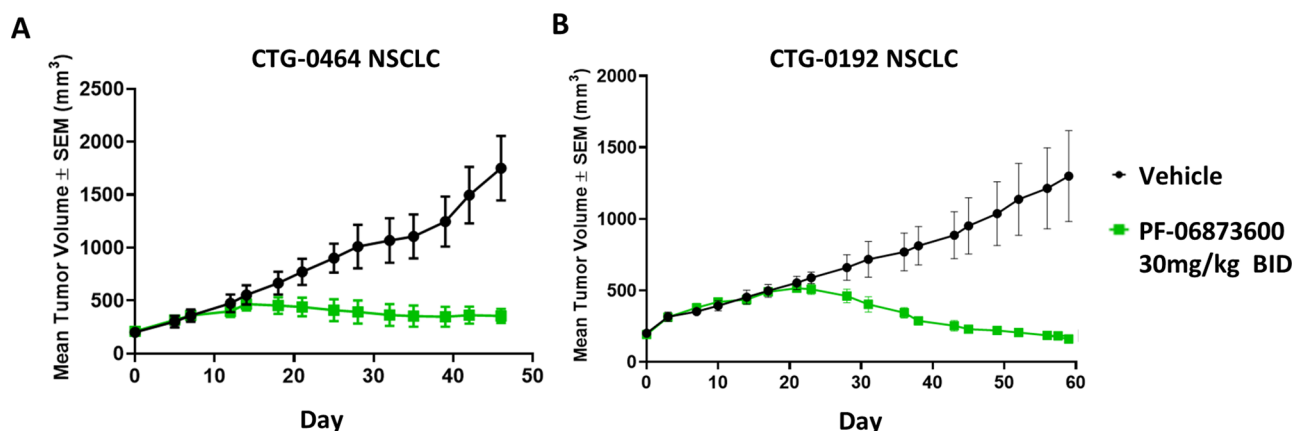
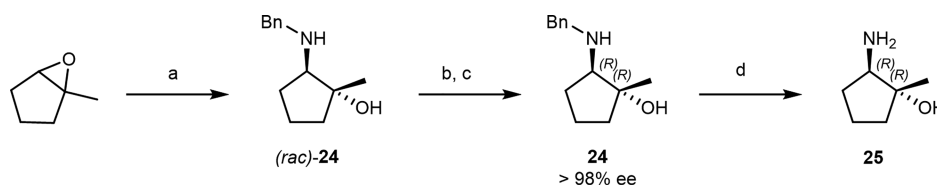


Figure 8. (A) *In vivo* tumor growth inhibition of **22** (PF-06873600) in PDX model CTG-0464 NSCLC. (B) *In vivo* tumor growth inhibition of **22** in PDX model CTG-0192 NSCLC. Both models are run with a vehicle arm and a twice daily dose of **22** given orally at 30 mg/kg.

Scheme 1. Synthesis of (1R,2R)-2-Amino-1-methylcyclopentan-1-ol (25**)^a**



^a(a) BnNH₂ and H₂O, 100 °C, 66%; (b) (2S)-[(3,5-dinitrobenzoyl)amino](phenyl) ethanoic acid (0.5 equiv) and EtOH, 80 °C to rt overnight, 82%, 96% ee; (c) repeat step b, but with 1 equiv of (2S)-[(3,5-dinitrobenzoyl)amino](phenyl) ethanoic acid, 97%, 98% ee; and (d) 20% Pd(OH)₂/C H₂ (1 atm), and isopropanol, 23 °C.

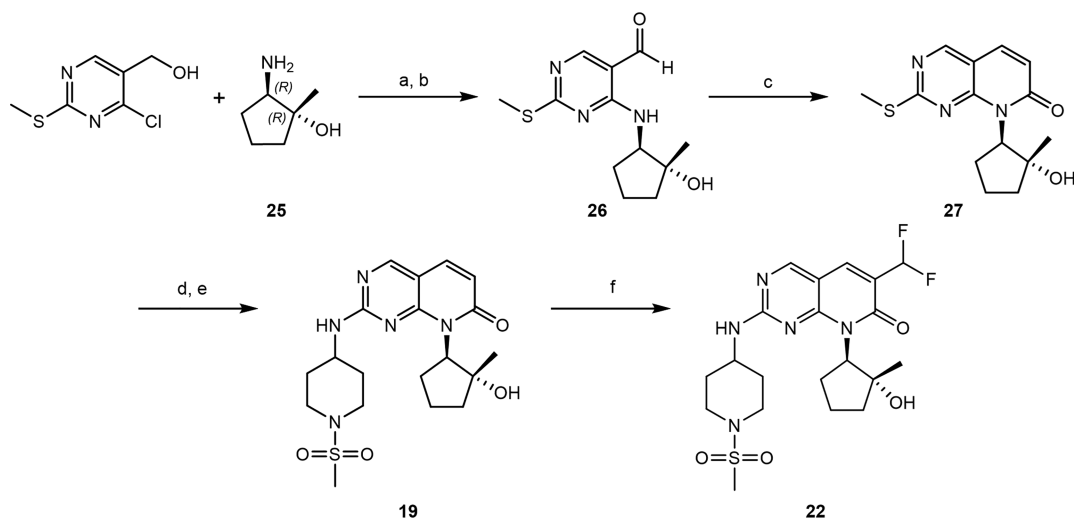
the 6-difluoromethyl substituent made van der Waals interactions with the sidechain phenyl of gatekeeper residue Phe80. Together, these interactions produced a potent and selective CDK2/4/6 inhibitor. More information on the biochemical profile of **22** is available in the [Supporting Information](#). This includes biochemical K_i data across a cohort of closely related CDK-family isoforms, and the related kinase GSK3 β . Additionally, it includes the results of kinase panel screening of **22** against 276 kinases.

Compound **22** provided the best combination of potency for CDK2, selectivity versus both CDK1 and CDK9, and low HLM Cl_{int} . Assessing the effects of CDK2 inhibition on cellular markers of CDK2 activity in an ovarian cancer cellular model (OVCAR3), compound **22** blocked the phosphorylation of RB1 with an EC_{50} of 19 nM and limited cell growth in this model with an EC_{50} of 45 nM for antiproliferation.⁴⁰ Notably, CDK4/6 inhibitors such as palbociclib (**1**) displayed no activity in these cells. In line with the measured biochemical selectivity, we measured the cellular CDK2 isoform engagement of **22** by the displacement of probe compound XO44³⁷ in triple negative breast cancer (HCC1806) cells (OC_{50} = 9 nM). In the same experiment, the engagement of CDK1 was also determined (OC_{50} = 597 nM). This ~60 \times isoform selectivity provided a compelling confirmation that a biochemical K_i ratio of 35 \times was similar to target engagement ratios in a cellular system.⁴⁰ Compound **22** also gave a strong phenotypic cellular response and arrested OVCAR3 cells in G1 at concentrations up to ~100 nM, and at higher concentrations generated a mixed population of G1 and G2 blocked cells.

Compound **22**, a neutral molecule, was anticipated to be absorbed mainly by the transcellular route based upon an analysis of physicochemical properties (SF log D at pH 7.4 = 1.9, molecular weight = 471.5, total polar surface area = 126,

hydrogen bond donor count = 2, and hydrogen bond acceptor count = 5) and solubility at pH 7.4 = 265 μ M. **22** demonstrated high passive permeability ($A/B \sim 14 \times 10^{-6}$ cm/s) *in vitro* in the RRCK(MDCK-LE) cell line, which was consistent with high transcellular absorption.⁴¹ In addition, after oral administration *in vivo* in mice and dogs, **22** exhibited high absorption ($f_a \cdot f_g \sim 1.0$ and 0.8) with time to maximal absorption (T_{max}) of 0.25 and 1 h, respectively. In an NSG strain of mice, **22** displayed a plasma clearance (CL_p) of 63 mL/min/kg, a volume of distribution (V_{ss}) of 0.9 L/kg, and an oral bioavailability (F) of 13%. Similarly, in beagle dogs, **22** showed a CL_p of 8.4 mL/min/kg, a V_{ss} of 1.1 L/kg, and an F of 59%. Based on these observed mean *in vivo* pharmacokinetic (PK) results in both mice and dogs, **22** was predicted to exhibit favorable oral drug properties in the clinic.

The pre-clinical *in vivo* anti-tumor activity for **22** was similarly promising. In mice-bearing OVCAR3 tumors, orally dosed **22** was shown to potently inhibit the phosphorylation of RB1 in the tumor cells, with an EC_{50} of 40 nM, and tumor growth inhibition studies showed 90% growth inhibition as a single agent at 50 mg per kg body weight with BID oral dosing.⁴⁰ CDK2 orchestrates progression through the cell cycle via the phosphorylation of RB1 when complexed with cyclin E or via the regulation of DNA synthesis and DNA repair machinery when complexed with cyclin A. Although modulation of RB1 phosphorylation tracks well with the efficacy and potency of **22**, we cannot rule out the fact that CDK2/cyclin A complexes also play a significant role in inhibitor function. Hyperactivation of cyclin E1/CDK2 signaling in tumors often occurs due to impaired cyclin E1 degradation pathways governed by the tumor suppressor E3 ligase FBXW7.^{42,43} FBXW7 is commonly mutated or deleted in a number of tumor types including non-small cell lung cancer

Scheme 2. Synthesis of 22 (PF-06873600)⁴⁴

^a(a) DIPEA and 2-propanol, 80 °C, 97%; (b) MnO₂ and EtOAc, 50 °C, 93%; (c) CH₃CO₂Et, LiHMDS, THF, -5 °C, EtOH, and AcOH, 71%; (d) oxone, 2-methyl-THF, and H₂O, 84%; (e) 1-(methylsulfonyl)piperidin-4-amine and 2-methyl-THF, 60 °C, 63%, >99% ee; and (f) CHF₂SO₂Na, t-BuOOH, FeCl₃/silica, DMSO, and H₂O, 57%.

(NSCLC), where 5% of patients present with homozygous deletions or loss of function mutation.⁴⁴ Figure 8 shows tumor growth inhibition studies performed in FBXW7 mutated PDX models of NSCLC, where 22 demonstrated 93% growth inhibition in the CTG-0464 model ($P < 0.001$) and 103% growth inhibition in the CTG-0192 model ($P < 0.001$).

CHEMISTRY

The synthesis of 22 is shown in Schemes 1 and 2. Scheme 1 describes the preparation of the chiral amino methylcyclopentanol (25), which was identified in the Free-Wilson analysis and is used in the 8-position of the pyridopyrimidinone ring system to provide potency and modulate lipophilicity. This route begins with the commercially available epoxide of methylcyclopentene which is opened by heating with benzylamine to give racemic 24. A classical resolution of 24 with the 3,5-dinitrobenzamide derivative of 2-(*S*)-phenylglycine gave the desired stereoisomer in 96% ee, and this step can be repeated for further enhancement of enantiomeric purity (>98% ee). Finally, the benzyl group can be removed under standard Pd-catalyzed hydrogenative deprotection conditions to provide 25.⁴⁵

At this point, compound 25 is reacted with commercially available [4-chloro-2-(methylthio)pyrimidin-5-yl]methanol (Scheme 2). Following S_NAr displacement of the chlorine, the resulting intermediate which contains a primary alcohol is oxidized with MnO₂ to give aldehyde 26 in 90% yield over 2 steps. With intermediates such as 26, there are several viable approaches to construct and further functionalize the pyridopyrimidinone core, including Horner-Wadsworth-Emmons methodology as reported previously.⁴⁶ In this work, the generation of the lithium enolate of ethyl acetate allowed carbon-carbon bond formation by condensation with aldehyde 26 and spontaneous ring closure during a quench with ethanol and acetic acid to form pyridopyrimidinone 27 in 71% yield.

Intermediates such as 27 also represent flexible precursors for final derivatization. The thioether at the 2-position of the pyridopyrimidinone system can be oxidized efficiently with

oxone to form a sulfone. The resulting 2-position sulfone is then subjected to S_NAr displacement with amines to give 2-aminopyridopyrimidinone analogues.^{47,48} In this sequence, this allows the installation of the amino-piperidine sulfonamide moiety to give 19, a compound which represented the first breakthrough result from the installation of (1*R*,2*R*)-2-amino-1-methylcyclopentanol-1-ol 25. To complete the synthesis of 22, a Langlois-Baran difluoromethyl functionalization reaction is utilized. In these reactions, a difluoromethyl radical is generated from a sulfinate precursor and *tert*-butyl hydroperoxide in the presence of iron or other inorganic counterions. In this system, the resultant difluoromethyl radical species reacts regioselectively at the 6-position of the pyridopyrimidinone core and provides 22 in 57% yield.^{49,50} Further details of these reactions, as well as synthetic experimental details for all compounds described in this work are available in the experimental section.

CONCLUSIONS

In summary, we have outlined a medicinal chemistry program that started with 2, a promising but relatively isoform nonselective lead for CDK2. This approach used a combination of structure-based drug design and property space analysis to design improved lead analogues, and a combination of cellular occupancy and mechanistic studies confirmed that these leads achieve the desired cellular functional effects. Free-Wilson analysis identified the highly efficient (1*R*,2*R*)-2-hydroxy-2-methylcyclopentyl moiety, which provided a key improvement in lipophilic efficiency that translated to both better potency as well as better metabolic stability. MD simulations were used to help understand the selectivity ratios observed between CDK2 and CDK9 and further refine the hypotheses around the structure-based drug design models. Subsequent modifications to improve the selectivity and ADME characteristics of these lead compounds provided advanced leads, including 22 (PF-06873600) which performed well in both *in vitro* and *in vivo* studies. PF-06873600 entered phase 1 clinical trials in 2018

and further communications regarding safety and efficacy will be reported in due course.

EXPERIMENTAL SECTION

General Methods. Unless otherwise noted, materials were obtained from commercial suppliers and were used without further purification. Unless otherwise stated, all reactions were performed under a positive pressure of nitrogen, argon, or with a drying tube; at ambient temperature; and in commercially purchased anhydrous solvents. Microwave-assisted reactions were run in a Biotage Initiator. Removal of the solvent under reduced pressure or concentration refers to distillation using a Büchi rotary evaporator attached to a vacuum pump (3 mm Hg). Products obtained as solids or high boiling oils were dried under vacuum (1 mm Hg) at ambient temperature, unless otherwise noted. Silica gel chromatography was performed on Teledyne Isco or Biotage purification systems using the manufacturer's pre-packed columns.

The reactions were assayed by high-performance liquid chromatography–mass spectrometry (LCMS) or thin-layer chromatography (TLC) and terminated as judged by the consumption of the starting material. Analytical TLC was performed on a glass-backed Silica gel 60 F₂₅₄ plates (Analtech, 0.25 mm) and eluted with the appropriate solvent ratios (v/v). The TLC plates were visualized by UV, *p*-anisaldehyde, phosphomolybdic acid, or iodine staining. LCMS utilized 254 and 220 nm wavelengths and either electrospray ionization (ESI) positive mode or atmospheric pressure chemical ionization (APCI) in positive mode.

¹H NMR spectra were recorded on a Bruker XWIN-NMR (400 or 700 MHz) spectrometer. Proton resonances are reported in parts per million (ppm) downfield from tetramethylsilane. ¹H NMR data are reported as multiplicity (s, singlet; d, doublet; t, triplet; q, quartet; quint, quintuplet; dd, doublet of doublets; dt, doublet of triplets; and br s, broad singlet). For spectra obtained in CDCl₃, DMSO-*d*₆, and CD₃OD, the residual protons (7.27, 2.50, and 3.31 ppm, respectively) were used as the internal reference. Optical rotations were determined on a JASCO P-2000 or a Rudolph Autopol IV polarimeter. All final compounds were purified to ≥ 95% purity, unless otherwise specified. For most compounds, purity was determined by Agilent 1200 or 1260 Series HPLCs coupled to an Agilent 6120 or 6140 Quadrupole LCMS with simultaneous UV (220 and 254 nm) and TIC detection (either APCI or ESI) or using a Shimadzu LC-20 HPLC with UV 220 nm detection.

Where specified, some analogues were synthesized as racemic mixtures with known relative stereochemistry and chiral preparative SFC was used to separate the enantiomers as the final stage. In these cases, absolute stereochemistry was not known for the separated enantiomers.

IUPAC names were generated from structures using ACD/Name 2017 software from ACD/Labs. When absolute stereochemistry is known, (*R,S*) labels are used. When absolute stereochemistry is not known, the software-generated names are modified to include (+)- and (−)-prefixes according to the optical rotations, and (*R**/*S**) labels are used to show relative configuration.

6-Acetyl-8-cyclopentyl-2-[[1-(methanesulfonyl)piperidin-4-yl]-amino]-5-methylpyrido[2,3-*d*]pyrimidin-7(8*H*)-one (2). Two parallel solutions of 6-acetyl-8-cyclopentyl-5-methyl-2-(methylthio)pyrido[2,3-*d*]pyrimidin-7(8*H*)-one⁴⁶ (29.0 g, 91.4 mmol each) in THF (300 mL each) and water (100 mL each) were treated with oxone (84.3 g, 137 mmol each) and stirred at rt for 1.5 h. The solutions were combined and filtered, and the filtrate was extracted with EtOAc (2 × 300 mL). The combined organics were washed with saturated aqueous NaCl, dried over sodium sulfate, filtered, and concentrated. The crude product was recrystallized with petroleum ether/EtOAc (20/1) to give 6-acetyl-8-cyclopentyl-2-(methanesulfonyl)-5-methylpyrido[2,3-*d*]pyrimidin-7(8*H*)-one (54.9 g, 42% for the combined batches) as a light yellow solid. ¹H NMR (400 MHz, CDCl₃): δ 9.11 (s, 1H), 5.88–5.92 (m, 1H), 3.38 (s, 3H), 2.56 (s, 3H), 2.45 (s, 3H), 2.24–2.29 (m, 2H), 2.14–2.15 (m, 2H), 1.95–1.96 (m, 2H), 1.70–1.72 (m, 2H); LCMS *m/z*: 350.1 [M + H]⁺. A

sealed tube containing a solution of 6-acetyl-8-cyclopentyl-2-(methanesulfonyl)-5-methylpyrido[2,3-*d*]pyrimidin-7(8*H*)-one (200 mg, 0.572 mmol), 1-(methylsulfonyl)piperidin-4-amine (133 mg, 0.744 mmol), and CsF (261 mg, 1.72 mmol) in DMSO (8 mL) was irradiated in a microwave at 140 °C for 15 min. After cooling to rt, the mixture was washed with water and extracted with CH₂Cl₂. The organic layer was dried over sodium sulfate, concentrated, and the residue recrystallized from methanol to give **2** (140 mg, 55%) as an orange solid. ¹H NMR (400 MHz, CDCl₃): δ 8.64 (s, 1H), 5.83 (quin, 1H, *J* = 8.8 Hz), 5.59–5.09 (m, 1H), 4.15–3.99 (m, 1H), 3.89–3.73 (m, 2H), 2.99–2.90 (m, 2H), 2.84 (s, 3H), 2.54 (s, 3H), 2.34 (s, 3H), 2.43–2.28 (m, 2H), 2.25–2.15 (m, 2H), 2.09–1.96 (m, 2H), 1.91–1.79 (m, 2H), 1.77–1.65 (m, 4H); ¹³C NMR (DMSO-*d*₆, 101 MHz): δ 202.4, 161.5, 161.2, 158.6, 155.7, 142.8, 128.6, 105.7, 53.3, 47.9, 44.7, 35.8, 31.6, 31.2, 28.1, 25.5, 13.8; HRMS: calcd for C₂₁H₂₉N₅O₄S (M + H)⁺, 448.2013; found, 448.20176.

8-Cyclopentyl-2-(methylthio)pyrido[2,3-*d*]pyrimidin-7(8*H*)-one. Two parallel batches were run using the following procedure, then combined for purification as noted below. To a solution of 4-(cyclopentylamino)-2-(methylthio)pyrimidine-5-carbaldehyde⁴⁶ (30.0 g, 130 mmol) in anhydrous THF (600 mL) was added EtOAc (33.4 g, 379 mmol) at −70 °C. The mixture was stirred at this temperature for 15 min, then LiHMDS (1.0 M in THF, 442 mL, 442 mmol) was added dropwise. The reaction was stirred at −70 °C for 30 min and then at rt (15 °C) for 16 h. The reaction mixture was slowly added to ice water (800 mL) and then extracted with EtOAc (3 × 500 mL). The combined organic layers were washed with saturated aqueous NH₄Cl (2 × 800 mL) and saturated aqueous NaCl (2 × 600 mL), dried over sodium sulfate, and concentrated. The crude products from both batches were combined and purified by silica gel chromatography (eluting with petroleum ether/EtOAc 10/1 to 5/1) to give 8-cyclopentyl-2-(methylthio)pyrido[2,3-*d*]pyrimidin-7(8*H*)-one (59.0 g, 87% combined yield) as a white solid. ¹H NMR (400 MHz, CDCl₃): δ 8.57 (s, 1H), 7.52 (d, 1H, *J* = 1.0 Hz), 6.58 (d, 1H, *J* = 1.0 Hz), 5.96–5.86 (m, 1H), 2.60 (s, 3H), 2.38–2.27 (m, 2H), 2.11–1.99 (m, 2H), 1.91–1.82 (m, 2H), 1.73–1.63 (m, 2H); LCMS *m/z*: 261.8 [M + H]⁺.

8-Cyclopentyl-2-[[1-(methanesulfonyl)piperidin-4-yl]amino]-pyrido[2,3-*d*]pyrimidin-7(8*H*)-one (3). Oxone (23.5 g, 38.3 mmol) was added to a cooled (0 °C) solution of 8-cyclopentyl-2-(methylthio)pyrido[2,3-*d*]pyrimidin-7(8*H*)-one (5.0 g, 19.13 mmol) in THF (100 mL) and water (20 mL), and the mixture was stirred at rt for 2 h. The mixture was diluted with EtOAc (300 mL), washed with water (100 mL), dried over sodium sulfate, and concentrated to give crude 8-cyclopentyl-2-(methanesulfonyl)pyrido[2,3-*d*]pyrimidin-7(8*H*)-one (5.40 g, 96%, ~90% purity) as a gray solid. LCMS *m/z*: 315.8 [M + H]⁺. A solution of this crude 8-cyclopentyl-2-(methanesulfonyl)pyrido[2,3-*d*]pyrimidin-7(8*H*)-one (5.40 g of ~90% purity, ~17.0 mmol), 1-(methylsulfonyl)piperidin-4-amine (5.34 g, 24.9 mmol), and DIPEA (14.7 mL, 82.8 mmol) in DMSO (70 mL) was stirred at 65 °C for 18 h. The reaction mixture was diluted with CH₂Cl₂ (150 mL), washed with saturated aqueous NH₄Cl (2 × 80 mL), dried over sodium sulfate, and concentrated to dryness. Recrystallization with 1/2 EtOAc/petroleum ether (50 mL) gave **3** (4.65 g, 72%) as a gray solid. ¹H NMR (400 MHz, DMSO-*d*₆): δ 8.68–8.54 (m, 1H), 7.88 (d, 1H, *J* = 6.3 Hz), 7.68 (d, 1H, *J* = 9.3 Hz), 6.28–6.16 (m, 1H), 5.92–5.74 (m, 1H), 4.02–3.82 (m, 1H), 3.58 (d, 2H, *J* = 10.8 Hz), 2.96–2.82 (m, 5H), 2.33 (d, 1H, *J* = 1.8 Hz), 2.19 (br s, 1H), 2.03–1.91 (m, 4H), 1.78–1.55 (m, 6H); ¹³C NMR (DMSO-*d*₆, 101 MHz): δ 163.5, 161.1, 159.5, 156.6, 136.7, 117.2, 105.9, 53.1, 47.8, 44.8, 35.7, 31.2, 28.0, 25.5; HRMS: calcd for C₁₈H₂₅N₅O₃S (M + H)⁺, 392.17509; found, 392.17586.

8-Cyclopentyl-6-methyl-2-(methylthio)pyrido[2,3-*d*]pyrimidin-7(8*H*)-one. To a solution of 4-(cyclopentylamino)-2-(methylthio)pyrimidine-5-carbaldehyde⁴⁶ (10.0 g, 42.1 mmol) in anhydrous THF (250 mL) was added ethyl propionate (12.9 g, 126 mmol) at −70 °C. The mixture was stirred at this temperature for 15 min, then LiHMDS (1.0 M in THF, 147 mL, 147 mmol) was added dropwise. The reaction was stirred at −70 °C for 30 min and then at rt (24 °C) for 16 h. At this time, TLC showed two product spots, which indicated

that a significant amount of the cyclized but not yet dehydrated intermediate, 8-cyclopentyl-5-hydroxy-6-methyl-2-(methylthio)-5,8-dihydropyrido[2,3-*d*]pyrimidin-7(6*H*)-one, was still present. The reaction mixture was partitioned between water and EtOAc (2 × 30 mL), and the combined organics were washed with aqueous NH₄Cl (30 mL) and saturated aqueous NaCl (30 mL), dried over sodium sulfate, filtered, and concentrated. To obtain the fully dehydrated product, the residue was dissolved in THF (200 mL), 1,8-diazabicyclo[5.4.0]undec-7-ene (7.06 g, 46.4 mmol) was added, and the mixture was heated to 60 °C for 3 h, at which time only the less polar product spot remained. The solution was diluted with EtOAc (200 mL) and washed with aqueous NH₄Cl (3 × 200 mL) and saturated aqueous NaCl (300 mL). The combined organics were dried over sodium sulfate and concentrated. The residue was suspended in 1:5 EtOAc/petroleum ether (100 mL), the solids collected by filtration and dried to give 8-cyclopentyl-6-methyl-2-(methylthio)pyrido[2,3-*d*]pyrimidin-7(8*H*)-one (11 g, 95%, ~90% purity by NMR) as a gray solid. ¹H NMR (400 MHz, CDCl₃): δ 8.50 (s, 1H), 7.40 (s, 1H), 5.94 (quin, 1H, *J* = 8.8 Hz), 2.56 (s, 3H), 2.34–2.27 (m, 2H), 2.17 (s, 3H), 2.08–2.00 (m, 2H), 1.86–1.83 (m, 2H), 1.68–1.65 (m, 2H).

8-Cyclopentyl-2-[[1-(methanesulfonyl)piperidin-4-yl]amino]-6-methylpyrido[2,3-*d*]pyrimidin-7(8*H*)-one (4). According to the sulfur oxidation and amine displacement methods described for the synthesis of 3, 8-cyclopentyl-6-methyl-2-(methylthio)pyrido[2,3-*d*]pyrimidin-7(8*H*)-one (2.50 g, 9.08 mmol), yielded, after final purification by silica gel chromatography, compound 4 (2.01 g, 54% 2-step yield) as a solid. ¹H NMR (400 MHz, DMSO-*d*₆, 80 °C): δ 8.49 (s, 1H), 7.51 (s, 1H), 7.27 (br s, 1H), 5.85 (quin, 1H, *J* = 8.7 Hz), 3.96 (br s, 1H), 3.62 (d, 2H, *J* = 12.0 Hz), 2.97–2.90 (m, 2H), 2.88 (s, 3H), 2.32 (br s, 2H), 2.04 (s, 3H), 2.03–1.92 (m, 4H), 1.83–1.72 (m, 2H), 1.72–1.54 (m, 4H); ¹³C NMR (DMSO-*d*₆, 101 MHz): δ 164.0, 160.6, 158.4, 155.7, 133.0, 125.0, 105.8, 53.3, 47.7, 44.8, 35.7, 31.3, 28.1, 25.6, 16.9; HRMS: calcd for C₁₉H₂₇N₃O₃S (M + H)⁺, 406.19704; found, 406.19115.

6-Chloro-8-cyclopentyl-2-[[1-(methanesulfonyl)piperidin-4-yl]amino]pyrido[2,3-*d*]pyrimidin-7(8*H*)-one (5). A solution of compound 3 (840 mg, 2.15 mmol) and *N*-chlorosuccinimide (315 mg, 2.36 mmol) in DMF (21.5 mL) was stirred at rt for 16 h and then at 70 °C for 4 h. The mixture was quenched with saturated aqueous NaHCO₃ (20 mL), causing a white solid to precipitate out. The precipitate was collected, dried, and then triturated in 1:1 EtOAc/heptane to give 5 (778 mg, 85%). ¹H NMR (400 MHz, DMSO-*d*₆, 80 °C): δ 8.59 (s, 1H), 8.01 (s, 1H), 7.65 (br s, 1H), 5.95–5.79 (m, 1H), 3.97 (br s, 1H), 3.61 (br d, 2H, *J* = 12.2 Hz), 2.96–2.84 (m, 5H), 2.28 (br s, 2H), 1.98 (br s, 4H), 1.80 (br s, 2H), 1.72–1.59 (m, 4H); ¹³C NMR (DMSO-*d*₆, 101 MHz): δ 161.0, 159.4, 159.3, 155.4, 134.6, 120.5, 105.2, 54.3, 47.9, 44.7, 35.7, 31.2, 28.1, 25.6; HRMS: calcd for C₁₈H₂₄ClN₃O₃S (M + H)⁺, 426.13611; found, 426.13662.

[8-Cyclopentyl-2-(methylthio)-7-oxo-7,8-dihydropyrido[2,3-*d*]pyrimidin-6-yl]acetic Acid. Diethyl succinate (44.0 g, 253 mmol) was added dropwise to a cooled (–70 °C) solution of LiHMDS (1.0 M in THF, 506 mL, 506 mmol) in THF (400 mL). After stirring for 10 min, a solution of 4-(cyclopentylamino)-2-(methylthio)pyrimidine-5-carbaldehyde⁴⁶ (40 g, 170 mmol) in THF (80 mL) was added. The reaction was stirred at –70 °C for 30 min, then at rt overnight. The mixture was diluted with water (1 L) and EtOAc (1 L), stirred for 10 min, then the layers were separated. The aqueous layer was further extracted with EtOAc (2 × 500 mL). No product was observed in the combined organic layers by TLC. The aqueous layer was acidified to pH 2 with conc. HCl. The resulting precipitate was collected by suction filtration, washed with water and petroleum ether, dried under vacuum, and then purified by silica gel chromatography (eluting with 2–5% MeOH in CH₂Cl₂) to give [8-cyclopentyl-2-(methylthio)-7-oxo-7,8-dihydropyrido[2,3-*d*]pyrimidin-6-yl]acetic acid (32 g, 59%) as a solid. ¹H NMR (400 MHz, DMSO-*d*₆): δ 12.36 (br s, 1H), 8.87 (s, 1H), 7.84 (s, 1H), 5.86 (quin, 1H, *J* = 8.8 Hz), 3.49 (s, 2H), 2.58 (s, 3H), 2.21–2.13 (m, 2H), 2.00–1.90 (m, 2H), 1.85–1.75 (m, 2H), 1.68–1.55 (m, 2H).

(8-Cyclopentyl-2-[[1-(methanesulfonyl)piperidin-4-yl]amino]-7-oxo-7,8-dihydropyrido[2,3-*d*]pyrimidin-6-yl]acetoneitrile (6). A suspension of [8-cyclopentyl-2-(methylthio)-7-oxo-7,8-dihydropyrido[2,3-*d*]pyrimidin-6-yl]acetic acid (5.00 g, 15.7 mmol) in EtOH (80 mL) was treated with conc. sulfuric acid (5 mL) and heated to 80 °C for 18 h, affording a clear yellow solution. After cooling to rt, the solution was concentrated to dryness, the residue was dissolved in CH₂Cl₂ (100 mL) and basified to pH ~8 with saturated aqueous Na₂CO₃. The layers were separated, and the aqueous layer further extracted with CH₂Cl₂ (2 × 50 mL). The combined organics were dried over sodium sulfate, filtered, concentrated, and purified by silica gel chromatography (eluting with 0–20% EtOAc in CH₂Cl₂) to give ethyl 2-(8-cyclopentyl-2-(methylthio)-7-oxo-7,8-dihydropyrido[2,3-*d*]pyrimidin-6-yl)acetate (4.90 g, 90%) as a yellow solid. A portion of this solid (3.00 g, 8.63 mmol) was treated with oxone by the method described for the synthesis of 3, affording 3.28 g of a crude mixture of sulfoxide (LCMS *m/z*: 364.1 [M + H]⁺, ~70%) and sulfone (LCMS *m/z*: 380.1 [M + H]⁺, ~30%) products, which were used without further purification. A portion of this mixture (500 mg, 1.32 mmol) was reacted with 1-(methylsulfonyl)piperidin-4-amine by the method described for the synthesis of 3, affording crude ethyl (8-cyclopentyl-2-[[1-(methanesulfonyl)piperidin-4-yl]amino]-7-oxo-7,8-dihydropyrido[2,3-*d*]pyrimidin-6-yl)acetate (260 mg, 41%) as a yellow gum. A solution of this gum (260 mg, 0.54 mmol) in ethanol (6 mL) was sparged with anhydrous ammonia gas for 10 min, the resulting solution stirred at 100 °C for 12 h, and then at 120 °C for an additional 12 h. The solution was concentrated to give 200 mg of crude 2-(8-cyclopentyl-2-[[1-(methanesulfonyl)piperidin-4-yl]amino]-7-oxo-7,8-dihydropyrido[2,3-*d*]pyrimidin-6-yl)acetamide (LCMS *m/z*: 449.0 [M + H]⁺, ~60%) as a mixture with unreacted starting ester (LCMS *m/z*: 478.0 [M + H]⁺, ~40%). A portion of this crude mixture (100 mg, ~0.13 mmol amide) dissolved in CH₂Cl₂ (5 mL) and cooled to 0 °C was treated with triethylamine (67.7 mg, 0.67 mmol) and trifluoroacetic acid anhydride (56.2 mg, 0.27 mmol). The cooling bath was removed, and the mixture stirred at rt for 2 h. The resulting yellow suspension was washed with deionized water (20 mL) and saturated aqueous NaCl. The organic layer was dried over magnesium sulfate, filtered, and concentrated. This crude product was combined with the crude product from a parallel run (starting with 80 mg, 0.11 mmol, of crude amide) for purification by preparative HPLC [column: DuraShell 150*25mm*5 μm; mobile phase: from 36 to 56% acetonitrile in H₂O (0.05% ammonium hydroxide v/v)] to give 6 (27.1 mg, 26% yield for the combined batches) as a white solid. ¹H NMR (400 MHz, DMSO-*d*₆, 80 °C): δ 8.65 (s, 1H), 7.80 (t, 1H, *J* = 0.9 Hz), 7.57 (br d, 1H, *J* = 7.3 Hz), 5.85 (quin, 1H, *J* = 8.9 Hz), 4.06–3.93 (m, 1H), 3.70 (d, 2H, *J* = 1.0 Hz), 3.62 (td, 2H, *J* = 3.4, 12.4 Hz), 2.96–2.89 (m, 2H), 2.88 (s, 3H), 2.37–2.24 (m, 2H), 2.08–1.95 (m, 4H), 1.86–1.74 (m, 2H), 1.73–1.59 (m, 4H); LCMS *m/z*: 430.9 [M + H]⁺.

8-Cyclopentyl-6-(hydroxymethyl)-2-[[1-(methanesulfonyl)piperidin-4-yl]amino]pyrido[2,3-*d*]pyrimidin-7(8*H*)-one (7). A suspension of 8-cyclopentyl-6-(ethoxymethyl)-2-[[1-(methanesulfonyl)piperidin-4-yl]amino]pyrido[2,3-*d*]pyrimidin-7(8*H*)-one (10) (100 mg, 0.22 mmol) and methane sulfonic acid (150 μL, 2.2 mmol) in acetonitrile (3.0 mL) and water (3.0 mL) was heated to 85 °C overnight. After cooling to rt, the mixture was quenched with saturated aqueous NaHCO₃, extracted with CH₂Cl₂ (4 × 10 mL), dried over sodium sulfate, concentrated, and purified by preparative SFC [ZymorSpher Diol Monol 150 × 21.2 mm column; gradient of 10–25% MeOH @ 3%/min, 100 bar, 58 mL/min] to give 7 (15.7 mg, 17%) as a solid. ¹H NMR (400 MHz, DMSO-*d*₆, 80 °C): δ 8.59 (s, 1H), 7.64 (s, 1H), 7.33 (br s, 1H), 5.85 (quin, 1H, *J* = 8.8 Hz), 4.79 (br s, 1H), 4.36 (br s, 2H), 3.98 (br s, 1H), 3.66–3.58 (m, 2H), 2.96–2.90 (m, 2H), 2.88 (s, 3H), 2.40–2.25 (m, 2H), 2.07–1.95 (m, 4H), 1.85–1.73 (m, 2H), 1.72–1.60 (m, 4H); LCMS *m/z*: 422.2 [M + H]⁺.

8-Cyclopentyl-6-(2-hydroxyethyl)-2-(methylthio)pyrido[2,3-*d*]pyrimidin-7(8*H*)-one. By the procedure described for 8-cyclopentyl-2-(methylthio)pyrido[2,3-*d*]pyrimidin-7(8*H*)-one but using ethyl 4-hydroxybutanoate instead of EtOAc, 6.0 g of 4-(cyclopentylamino)-2-

(methylthio)pyrimidine-5-carbaldehyde was used to produce 8-cyclopentyl-6-(2-hydroxyethyl)-2-(methylthio)pyrido[2,3-*d*]-pyrimidin-7(8*H*)-one (5.98 g, 77%) as a yellow solid. ¹H NMR (400 MHz, CDCl₃): δ 8.57 (s, 1H), 7.49 (s, 1H), 5.96 (quin, 1H, *J* = 8.8 Hz), 3.89 (t, 2H, *J* = 5.8 Hz), 2.87 (t, 2H, *J* = 5.6 Hz), 2.73 (br s, 1H), 2.61 (s, 3H), 2.38–2.26 (m, 2H), 2.13–2.01 (m, 2H), 1.94–1.83 (m, 2H), 1.73–1.62 (m, 2H); LCMS *m/z*: 305.8 [M + H]⁺.

8-Cyclopentyl-6-(2-hydroxyethyl)-2-[[1-(methanesulfonyl)piperidin-4-yl]amino]pyrido[2,3-*d*]pyrimidin-7(8*H*)-one (8). According to the method described for the synthesis of 3, 8-cyclopentyl-6-(2-hydroxyethyl)-2-(methylthio)pyrido[2,3-*d*]pyrimidin-7(8*H*)-one was used to produce 8 (342 mg, 61% 2-step yield) as a light yellow solid. ¹H NMR (400 MHz, DMSO-*d*₆, 80 °C): δ 8.52 (s, 1H), 7.51 (s, 1H), 7.34 (br d, 1H, *J* = 7.6 Hz), 5.85 (quin, 1H, *J* = 9.0 Hz), 4.29 (br s, 1H), 4.02–3.90 (m, 1H), 3.66–3.54 (m, 4H), 2.93–2.87 (m, 5H), 2.62 (t, 2H, *J* = 6.8 Hz), 2.37–2.24 (m, 2H), 2.06–1.93 (m, 4H), 1.82–1.71 (m, 2H), 1.71–1.58 (m, 4H); ¹³C NMR (DMSO-*d*₆, 101 MHz): δ 163.8, 160.6, 158.7, 155.6, 133.6, 126.5, 105.8, 60.2, 53.3, 47.8, 44.8, 35.7, 34.2, 31.3, 28.1, 25.6; HRMS: calcd for C₂₀H₂₉N₅O₄S (M + H)⁺, 436.2013; found, 436.20155.

8-Cyclopentyl-2-[[1-(methanesulfonyl)piperidin-4-yl]amino]-6-(2-methoxyethyl)pyrido[2,3-*d*]pyrimidin-7(8*H*)-one (9). According to the cyclization method described for the synthesis of 8-cyclopentyl-2-(methylthio)pyrido[2,3-*d*]pyrimidin-7(8*H*)-one, methyl 4-methoxybutanoate (668 mg, 5.1 mmol) and 4-(cyclopentylamino)-2-(methylthio)pyrimidine-5-carbaldehyde⁴⁶ (400 mg, 1.69 mmol) afforded 8-cyclopentyl-6-(2-methoxyethyl)-2-(methylthio)pyrido[2,3-*d*]pyrimidin-7(8*H*)-one (428 mg, 79%) as a yellow gum. LCMS *m/z*: 319.9 [M + H]⁺. All of this material was subjected to the sulfur oxidation and amine displacement methods previously described for the synthesis of 3, affording compound 9 (70.73 mg, 11.7% 2-step yield) as a yellow solid, after silica gel chromatography (eluting with 1% MeOH in CH₂Cl₂) and lyophilization. ¹H NMR (400 MHz, CDCl₃): δ 8.38 (s, 1H), 7.38 (s, 1H), 5.88 (quin, 1H, *J* = 8.8 Hz), 5.23 (br s, 1H), 4.03 (br d, 1H, *J* = 7.0 Hz), 3.80 (br d, 2H, *J* = 12.0 Hz), 3.65 (t, 2H, *J* = 6.1 Hz), 3.36 (s, 3H), 3.01–2.89 (m, 2H), 2.87–2.79 (m, 5H), 2.35 (br s, 2H), 2.20 (br dd, 2H, *J* = 3.1, 13.4 Hz), 2.10–1.99 (m, 2H), 1.92–1.79 (m, 2H), 1.76–1.63 (m, 4H); ¹³C NMR (DMSO-*d*₆, 101 MHz): δ 163.6, 160.7, 158.8, 155.7, 133.7, 125.9, 105.7, 70.9, 58.1, 53.3, 47.8, 44.8, 35.7, 31.3, 30.6, 28.1, 25.6; HRMS: calcd for C₂₁H₃₁N₅O₄S (M + H)⁺, 450.21695; found, 450.21791.

8-Cyclopentyl-6-(ethoxymethyl)-2-(methylthio)pyrido[2,3-*d*]pyrimidin-7(8*H*)-one. By the procedure described for 8-cyclopentyl-2-(methylthio)pyrido[2,3-*d*]pyrimidin-7(8*H*)-one but using ethyl 3-ethoxypropanoate instead of EtOAc, 1.00 g of 4-(cyclopentylamino)-2-(methylthio)pyrimidine-5-carbaldehyde⁴⁶ produced 8-cyclopentyl-6-(ethoxymethyl)-2-(methylthio)pyrido[2,3-*d*]pyrimidin-7(8*H*)-one (406 mg, 60%) as a white solid. ¹H NMR (400 MHz, CDCl₃): δ 8.63 (s, 1H), 7.68 (t, 1H, *J* = 1.6 Hz), 5.98 (quin, 1H, *J* = 8.9 Hz), 4.49 (d, 2H, *J* = 1.5 Hz), 3.74–3.65 (m, 2H), 2.63 (s, 3H), 2.40–2.27 (m, 2H), 2.16–2.03 (m, 2H), 1.97–1.84 (m, 2H), 1.76–1.65 (m, 2H), 1.32 (t, 3H, *J* = 7.0 Hz); LCMS *m/z*: 319.9 [M + H]⁺.

8-Cyclopentyl-6-(ethoxymethyl)-2-[[1-(methanesulfonyl)piperidin-4-yl]amino]pyrido[2,3-*d*]pyrimidin-7(8*H*)-one (10). A solution of oxone (4.58 g, 7.45 mmol) in water (40 mL) was added to a cooled (0 °C) solution of 8-cyclopentyl-6-(ethoxymethyl)-2-(methylthio)pyrido[2,3-*d*]pyrimidin-7(8*H*)-one (1.19 g, 3.73 mmol) in THF (37.3 mL). The resulting suspension was stirred and allowed to slowly warm to rt over 1 h. More water (20 mL) was added, and the precipitate was collected and dried to give 8-cyclopentyl-6-(ethoxymethyl)-2-(methanesulfonyl)pyrido[2,3-*d*]pyrimidin-7(8*H*)-one (933 mg, 71%) as a solid. ¹H NMR (400 MHz, CDCl₃): δ 8.96 (s, 1H), 7.86 (t, 1H, *J* = 1.7 Hz), 5.97 (quin, 1H, *J* = 8.7 Hz), 4.54 (d, 2H, *J* = 1.7 Hz), 3.72 (q, 2H, *J* = 7.0 Hz), 3.39 (s, 3H), 2.38–2.23 (m, 2H), 2.24–2.12 (m, 2H), 2.06–1.87 (m, 2H), 1.78–1.64 (m, 2H), 1.34 (t, 3H, *J* = 7.0 Hz). A mixture of 8-cyclopentyl-6-(ethoxymethyl)-2-(methanesulfonyl)pyrido[2,3-*d*]pyrimidin-7(8*H*)-one (933 mg, 2.65 mmol), 1-(methylsulfonyl)piperidin-4-amine (855 mg, 3.98 mmol), and DIPEA (1.39 mL, 7.96 mmol) in DMSO (13.3

mL) was stirred at rt for 2 days, then at 60 °C for 4 h. Water (20 mL) was added, which caused a precipitate to form. The resulting solid was collected by filtration and dried in a 50 °C vacuum oven for 1 day, affording 10 (752 mg, 63%) as a light yellow solid. ¹H NMR (400 MHz, DMSO-*d*₆, 80 °C): δ 8.60 (s, 1H), 7.63 (s, 1H), 7.37 (d, 1H, *J* = 7.3 Hz), 5.84 (quin, 1H, *J* = 8.9 Hz), 4.32 (d, 2H, *J* = 1.0 Hz), 4.06–3.90 (m, 1H), 3.70–3.52 (m, 4H), 2.96–2.89 (m, 2H), 2.88 (s, 3H), 2.39–2.23 (m, 2H), 2.06–1.96 (m, 4H), 1.85–1.73 (m, 2H), 1.72–1.57 (m, 4H), 1.20 (t, 3H, *J* = 7.0 Hz); ¹³C NMR (151 MHz, DMSO-*d*₆, 70 °C): δ 161.8, 160.0, 158.7, 154.9, 131.8, 124.9, 104.7, 66.5, 65.3, 52.3, 46.9, 44.0, 34.7, 30.4, 27.3, 24.8, 14.7; HRMS: calcd for C₂₁H₃₁N₅O₄S [M + H]⁺, 450.2170; found 450.2177.

Ethyl 3-(cyclopropyloxy)propanoate. To a solution of cyclopropanol (5 g, 90 mmol) and ethyl acrylate (13.8 g, 138 mmol) in DMSO (50 mL) was added 5 M aqueous NaOH solution (1.72 mL, 8.6 mmol) dropwise. The solution color changed from yellow to blue and back to yellow again during the addition. Stirring was continued at rt (16 °C) for 48 h. The mixture was partitioned between EtOAc (150 mL) and water (100 mL). The aqueous layer was further extracted with MTBE (3 × 100 mL). The combined organic phases were washed with water (3 × 100 mL) and saturated aqueous NaCl (100 mL), dried over sodium sulfate, filtered, and concentrated to a light-yellow liquid. Purification by silica gel chromatography (eluting with 0–10% EtOAc in petroleum ether) afforded ethyl 3-(cyclopropyloxy)propanoate (8.0 g, 59%, ~90% purity) as colorless liquid. ¹H NMR (400 MHz, CDCl₃): δ 4.15 (q, 2H, *J* = 7.1 Hz), 3.77 (t, 2H, *J* = 6.4 Hz), 3.29 (tt, 1H, *J* = 3.0, 6.0 Hz), 2.56 (t, 2H, *J* = 6.4 Hz), 1.26 (t, 3H, *J* = 7.1 Hz), 0.59–0.53 (m, 2H), 0.48–0.41 (m, 2H).

8-Cyclopentyl-6-[(cyclopropyloxy)methyl]-2-[[1-(methanesulfonyl)piperidin-4-yl]amino]pyrido[2,3-*d*]pyrimidin-7(8*H*)-one (11). A three-necked flask containing a solution of 4-(cyclopentylamino)-2-(methylthio)pyrimidine-5-carbaldehyde⁴⁶ (150 mg, 0.632 mmol) and ethyl 3-(cyclopropyloxy)propanoate (300 mg, 1.9 mmol) in freshly distilled anhydrous THF (5 mL) under argon was cooled in an ice–water bath. A 1 M solution of NaHMDS in THF (1.9 mL, 1.9 mmol) was added dropwise over 2 min, slowly enough to maintain the internal temperature below 3 °C. The resulting turbid mixture was stirred at this temperature for 40 min, quenched with aqueous NH₄Cl (0.5 mL), and stirring was continued at rt (25 °C) overnight. The solution was concentrated and purified by silica gel chromatography (eluting with 0–10% EtOAc in petroleum ether) to give a 2:1 mixture of 8-cyclopentyl-6-[(cyclopropyloxy)methyl]-2-(methylthio)pyrido[2,3-*d*]pyrimidin-7(8*H*)-one and unreacted aldehyde starting material (120 mg combined). LCMS *m/z*: 332.2 [M + H]⁺. A solution of this mixture in THF (6 mL) was treated with oxone (334 mg, 0.543 mmol) and water (1 mL) and stirred at rt (28 °C) for 1 h. The mixture was partitioned between EtOAc (10 mL) and saturated aqueous NaCl (3 mL). The organic layer was dried over sodium sulfate, filtered, and concentrated to give crude 8-cyclopentyl-6-[(cyclopropyloxy)methyl]-2-(methanesulfonyl)pyrido[2,3-*d*]pyrimidin-7(8*H*)-one (130 mg) as a yellow gum. This crude product was dissolved in DMSO (1 mL) in a sealed tube. DIPEA (0.187 mL, 1.07 mmol) and 1-(methylsulfonyl)piperidin-4-amine (130 mg, 0.729 mmol) were added, the tube was sealed, and the mixture was heated at 60 °C for 1.5 h. After standing at rt overnight, excess DIPEA was removed by a syringe. The DMSO phase was diluted with CH₂Cl₂ (30 mL), washed with water (10 mL), aqueous NH₄Cl (10 mL), and saturated aqueous NaCl (10 mL), dried over sodium sulfate, filtered, and concentrated. The crude product was purified by silica gel chromatography (eluting with 0–10% EtOAc in CH₂Cl₂) and then lyophilized to give 11 (42.4 mg, 15% over 3 steps) as a pale solid. ¹H NMR (400 MHz, DMSO-*d*₆, 80 °C): δ 8.60 (s, 1H), 7.70–7.57 (m, 1H), 7.43 (br d, 1H, *J* = 6.2 Hz), 5.84 (quin, 1H, *J* = 8.8 Hz), 4.37 (d, 2H, *J* = 1.1 Hz), 4.04–3.91 (m, 1H), 3.61 (td, 2H, *J* = 3.4, 12.4 Hz), 3.42 (tt, 1H, *J* = 3.0, 6.0 Hz), 2.96–2.89 (m, 2H), 2.88 (s, 3H), 2.38–2.25 (m, 2H), 2.06–1.95 (m, 4H), 1.83–1.73 (m, 2H), 1.72–1.59 (m, 4H), 0.60–0.42 (m, 4H); LCMS *m/z*: 462.0 [M + H]⁺.

6-Bromo-8-cyclopentyl-2-[[1-(methanesulfonyl)piperidin-4-yl]amino]pyrido[2,3-d]pyrimidin-7(8H)-one. A solution of 8-cyclopentyl-2-(methylthio)pyrido[2,3-d]pyrimidin-7(8H)-one (20.0 g, 76.5 mmol) and *N*-bromosuccinimide (20.4 g, 115 mmol) in acetonitrile (160 mL) and CH₂Cl₂ (160 mL) was stirred at 50 °C for 17 h. The mixture was concentrated to dryness, affording a crude mixture of 6-bromo-8-cyclopentyl-2-(methylthio)pyrido[2,3-d]pyrimidin-7(8H)-one and 6-bromo-8-cyclopentyl-2-(methanesulfonyl)pyrido[2,3-d]pyrimidin-7(8H)-one. (38 g total, yellow solid). LCMS *m/z*: 341.9 and 358.0 [M + H]⁺, both Br doublets. The crude product mixture was dissolved in THF (350 mL) and water (175 mL), oxone (94.1 g, 153 mmol) was added, and the mixture was stirred at 50 °C for 11 h. After standing at rt overnight, the reaction mixture was concentrated to dryness, and the residue was partitioned between water (500 mL) and EtOAc (3 × 300 mL). The combined organics were washed with saturated aqueous NaCl (300 mL), dried over sodium sulfate, filtered, concentrated, and purified by silica gel chromatography (eluting with 0–60% EtOAc in petroleum ether) to give 16.5 g of a yellow solid, still contaminated with succinimide. This solid was dissolved in CH₂Cl₂ (500 mL), washed with saturated aqueous sodium carbonate (2 × 200 mL) and saturated aqueous NaCl (200 mL), dried over sodium sulfate, filtered, and concentrated. The residue was triturated with CH₂Cl₂ (5 mL) and MTBE (100 mL). The solid was collected by filtration and dried to give 6-bromo-8-cyclopentyl-2-(methanesulfonyl)pyrido[2,3-d]pyrimidin-7(8H)-one (15 g, 53% 2-step yield) as a white solid. ¹H NMR (400 MHz, CDCl₃): δ 8.94 (s, 1H), 8.20 (s, 1H), 6.02 (quin, 1H, *J* = 7.8), 3.40 (s, 3H), 2.26–2.17 (m, 4H), 1.99–1.97 (m, 2H), 1.74–1.71 (m, 2H); LCMS *m/z*: 373.8 [M + H]⁺. A portion of this sulfone intermediate (1.31 g, 3.519 mmol) was reacted with 1-(methylsulfonyl)piperidin-4-amine by the method described for the synthesis of 3, to give 6-bromo-8-cyclopentyl-2-[[1-(methanesulfonyl)piperidin-4-yl]amino]pyrido[2,3-d]pyrimidin-7(8H)-one (1.07 g, 65%) as a yellow solid. ¹H NMR (400 MHz, DMSO-*d*₆, 80 °C): δ 8.60 (s, 1H), 8.20 (s, 1H), 7.64 (d, 1H, *J* = 7.0 Hz), 5.89 (quin, 1H, *J* = 8.7 Hz), 3.99 (d, 1H, *J* = 6.4 Hz), 3.73–3.52 (m, 2H), 2.98–2.90 (m, 2H), 2.89 (s, 3H), 2.35–2.21 (m, 2H), 2.06–1.95 (m, 4H, *J* = 8.8 Hz), 1.87–1.76 (m, 2H), 1.74–1.61 (m, 4H); LCMS *m/z*: 471.65/469.75 [M + H]⁺ (Br doublet).

8-Cyclopentyl-2-[[1-(methanesulfonyl)piperidin-4-yl]amino]-6-[[propan-2-yl]oxy]methyl]pyrido[2,3-d]pyrimidin-7(8H)-one (12). In a microwave vial, a solution of 6-bromo-8-cyclopentyl-2-[[1-(methanesulfonyl)piperidin-4-yl]amino]pyrido[2,3-d]pyrimidin-7(8H)-one (50 mg, 0.11 mmol), potassium isopropoxymethyltrifluoroborate (190 mg, 1.06 mmol), [1,1'-bis(diphenylphosphino)ferrocene]dichloropalladium(II) (5.06 mg, 0.0069 mmol), and potassium phosphate (tribasic, 1 mL of a 7 M aqueous solution, 7 mmol) in THF (10 mL) was purged with nitrogen gas for 5 min, then irradiated in a microwave reactor at 100 °C for 6 h. After cooling to rt, the mixture was partitioned between water (5 mL) and CH₂Cl₂ (5 × 5 mL). The combined organics were concentrated to dryness and purified by preparative SFC [ZymorSpher Pyridine Diol 150 × 21.2 mm column; gradient of 5–15% MeOH @ 3%/min then ramped to 15–40% MeOH at 99%/min, 100 bar, 58 mL/min] to give 12 (12.8 mg, 26%) as a solid. ¹H NMR (400 MHz, CDCl₃, 80 °C): δ 8.61 (s, 1H) 7.63 (s, 1H) 7.30–7.47 (m, 1H) 5.68–5.97 (m, 1H) 4.32 (d, 2H, *J* = 1.2 Hz) 3.89–4.06 (m, 1H) 3.72 (d, 1H, *J* = 6.1 Hz) 3.63 (d, 2H, *J* = 12.5 Hz) 2.93 (br s, 2H) 2.88 (s, 3H) 2.25–2.39 (m, 2H) 1.95–2.08 (m, 4H) 1.74–1.85 (m, 2H) 1.67 (d, 4H, *J* = 10.2 Hz) 1.19 (d, 6H, *J* = 6.1 Hz); LCMS *m/z*: 464.2 [M + H]⁺.

4-(Cycloheptylamino)-2-(methylthio)pyrimidine-5-carbaldehyde. A suspension of ethyl 4-chloro-2-(methylthio)pyrimidine-5-carboxylate (16 g, 68.7 mmol), cycloheptylamine (9.34 g, 82.5 mmol), and DIPEA (17.8 g, 138 mmol) in THF (150 mL) was stirred at rt for 18 h. Solvents were evaporated, the residue dissolved in water (150 mL), and the solution extracted with EtOAc (2 × 150 mL). The combined organics were washed with saturated aqueous NaCl (2 × 150 mL), dried over sodium sulfate, and concentrated to give ethyl 4-(cycloheptylamino)-2-(methylthio)pyrimidine-5-carboxylate (21 g, 99%) as yellow oil. LCMS *m/z*: 309.9 [M + H]⁺. A cooled (5 °C)

solution of ethyl 4-(cycloheptylamino)-2-(methylthio)pyrimidine-5-carboxylate (21 g, 67.9 mmol) in THF (200 mL) was treated with lithium aluminum hydride (2.5 M solution in THF, 81.4 mL, 204 mmol) in portions over 1.5 h. The resulting suspension was stirred at 5–10 °C for an additional hour, then at rt (25 °C) for 18 h. The mixture was cooled slightly (15 °C), then water (10 mL) and 2 N NaOH (10 mL) were added dropwise to quench any residual hydride. After stirring for 1 h at rt, the suspension was filtered, and the flask and filter cake were rinsed with THF (4 × 300 mL). The combined filtrates were concentrated to remove most of the solvent, and the residue was partitioned between water (100 mL) and EtOAc (2 × 250 mL). The combined organic layers were washed with saturated aqueous NaCl (100 mL), dried over sodium sulfate, and concentrated to dryness. The crude product was recrystallized from petroleum ether/EtOAc (200 mL/50 mL) to give [4-(cycloheptylamino)-2-(methylthio)pyrimidin-5-yl]methanol (13.6 g, 75%) as a white solid. LCMS *m/z*: 267.9 [M + H]⁺. Activated manganese dioxide (43.3 g, 860 mmol) was added to a solution of [4-(cycloheptylamino)-2-(methylthio)pyrimidin-5-yl]methanol (13.6 g, 50 mmol) in chloroform (200 mL), and the resulting suspension stirred at rt for 15 h. The solids were removed by filtration. The flask and filter cake were rinsed with CH₂Cl₂ (4 × 150 mL). The combined filtrates were filtered again to remove trace solids, then concentrated to give 4-(cycloheptylamino)-2-(methylthio)pyrimidine-5-carbaldehyde (12.9 g, 98%) as yellow oil. ¹H NMR (400 MHz, CDCl₃): δ 9.68 (s, 1H), 8.63 (br s, 1H), 8.28 (s, 1H), 4.36–4.32 (m, 1H), 2.55 (s, 3H), 2.03–1.99 (m, 2H), 1.67–1.58 (m, 10H); LCMS *m/z*: 265.9 [M + H]⁺.

8-Cycloheptyl-2-(methylthio)pyrido[2,3-d]pyrimidin-7(8H)-one. By the same method used for 8-cyclopentyl-2-(methylthio)pyrido[2,3-d]pyrimidin-7(8H)-one but with an initial reaction temperature of –5 °C instead of –70 °C, 4-(cycloheptylamino)-2-(methylthio)pyrimidine-5-carbaldehyde (9.9 g, 37 mmol) was reacted with EtOAc (9.79 g, 111 mmol) and LiHMDS (111 mL of a 1.0 M solution in THF) to give, after silica gel chromatography, 8-cycloheptyl-2-(methylthio)pyrido[2,3-d]pyrimidin-7(8H)-one (9.5 g, 89%) as a yellow solid. ¹H NMR (400 MHz, CDCl₃): δ 8.57 (s, 1H), 7.52 (d, 1H, *J* = 9.6 Hz), 6.60 (br s, 1H), 5.72 and 5.44 (2 br s, 1H together), 2.75–2.51 (m, 5H), 1.95–1.62 (m, 10 H); LCMS *m/z*: 289.9 [M + H]⁺.

8-Cycloheptyl-2-[[1-(methanesulfonyl)piperidin-4-yl]amino]pyrido[2,3-d]pyrimidin-7(8H)-one (13). According to the two-step method described for the synthesis of 3, 8-cycloheptyl-2-(methylthio)pyrido[2,3-d]pyrimidin-7(8H)-one was used to produce 13 (107 mg, 37% 2-step yield) after a final purification by preparative SFC. ¹H NMR (700 MHz, DMSO-*d*₆): δ 8.50 (br s, 1H) 7.80 (br s, 1H) 7.59 (d, 1H, *J* = 9.2 Hz) 6.30–5.98 (m, 1H) 5.49 and 5.21 (2 br s, 1H together) 4.04–3.81 (m, 1H) 3.54 (br s, 2H) 2.84 (s, 3H) 2.79 (br s, 2H) 2.52 (d, 1H, *J* = 9.9 Hz) 2.31 (br s, 1H) 2.08–1.84 (m, 2H) 1.70 (br s, 2H) 1.62–1.32 (m, 10H); ¹³C NMR (101 MHz, DMSO-*d*₆, 80 °C): δ 162.26, 160.14, 158.45, 154.97, 135.78, 116.24, 104.85, 53.79, 47.18, 43.94, 34.87, 31.02, 30.28, 27.12, 25.88; HRMS: calculated for C₂₀H₂₉N₅O₃S [M + H]⁺, 420.2064; found 420.2070.

8-Cyclohexyl-2-[[1-(methanesulfonyl)piperidin-4-yl]amino]pyrido[2,3-d]pyrimidin-7(8H)-one (14). A mixture of 8-cyclohexyl-2-(methylthio)pyrido[2,3-d]pyrimidin-7(8H)-one⁴⁷ (60.0 mg, 0.206 mmol), 1-(methylsulfonyl)piperidin-4-amine (70.0 mg, 0.393 mmol), and cesium fluoride (59.7 mg, 0.393 mmol) in DMSO (3 mL, pre-treated with CaH₂) was irradiated in a microwave reactor at 140 °C for 15 min. After cooling to rt, the mixture was diluted with CH₂Cl₂ (30 mL) and washed with water (2 × 10 mL) and saturated aqueous NaCl (10 mL). The organics were dried over sodium sulfate, filtered, concentrated, purified by preparative TLC (MeOH/CH₂Cl₂ = 1/15), and lyophilized to give 14 (57.2 mg, 36%) as a yellow solid. ¹H NMR (400 MHz, CDCl₃): δ 8.38 (s, 1H), 7.40 (d, 1H), 6.37 (br s, 1H), 5.54 (br s, 1H), 5.40–5.25 (m, 1H), 4.05–3.95 (m, 1H), 3.83–3.81 (m, 2H), 3.00–2.90 (m, 2H), 2.85 (s, 3H), 2.75–2.60 (m, 2H), 2.24–2.21 (m, 2H), 1.90–1.85 (m, 2H), 1.73–1.68 (m, 5H), 1.42–1.25 (m, 3H); LCMS *m/z*: 406.0 [M + H]⁺.

2-[[1-(Methanesulfonyl)piperidin-4-yl]amino]-8-[(1R,2S)-2-methylcyclopentyl]pyrido[2,3-d]pyrimidin-7(8H)-one (**15**). Prepared by the same method as used for **13** but starting with (1R,2S)-2-methylcyclopentylamine.⁵¹ ¹H NMR (400 MHz, CDCl₃): δ 8.38 (s, 1H), 7.41 (d, 1H, J = 9.3 Hz), 6.34 (d, 1H, J = 9.3 Hz), 6.01–5.86 (m, 1H), 4.10–3.95 (m, 1H), 3.79 (d, 2H, J = 10.5 Hz), 2.93 (br s, 2H), 2.83 (s, 3H), 2.79–2.51 (m, 1H), 2.34 (br s, 1H), 2.19 (d, 2H, J = 12.3 Hz), 2.10–1.99 (m, 1H), 1.89 (dd, 4H, J = 7.7, 18.7 Hz), 1.76–1.61 (m, 2H), 1.60–1.45 (m, 1H), 0.78 (d, 3H, J = 7.0 Hz); ¹³C NMR (CDCl₃, 151 MHz): δ 164.5, 159.8, 157.5, 157.1, 135.3, 119.2, 106.3, 56.3, 47.8, 44.7, 38.0, 35.2, 35.1, 31.5, 28.0, 25.5, 15.1 95% ee by chiral analytical SFC/MS [Column: Chiralpak AD-3 100 × 4.6 mm I.D., 3 μm; Mobile phase: A: CO₂ B/ethanol (0.05% diethylamine); Gradient: from 5 to 40% of B in 4.5 min and hold 40%; for 2.5 min, then 5% of B for 1 min; Flow rate: 2.8 mL/min; 40 °C]; HRMS: calcd for C₁₉H₂₇N₅O₃S [M + H]⁺, 406.1835; found 406.1901.

rac-{4-[(Butan-2-yl)amino]-2-(methylthio)pyrimidin-5-yl}-methanol. A solution of [4-chloro-2-(methylthio)pyrimidin-5-yl]-methanol (500 mg, 2.62 mmol), (±)-butan-2-amine (249 mg, 3.41 mmol), and triethylamine (796 mg, 7.78 mmol) in ethanol (2 mL) and acetonitrile (2 mL) was stirred at 80 °C for 18 h. After cooling to rt, the mixture was diluted with CH₂Cl₂ (100 mL) and washed with aqueous NH₄Cl (50 mL) and saturated aqueous NaCl (50 mL). The organic layer was dried over sodium sulfate, filtered, concentrated, and purified by silica gel chromatography to give *rac*-{4-[(butan-2-yl)amino]-2-(methylthio)pyrimidin-5-yl}methanol (520 mg, 87%) as a light yellow solid. LCMS *m/z*: 227.8 [M + H]⁺.

rac 4-[(Butan-2-yl)amino]-2-(methylthio)pyrimidine-5-carbaldehyde. Activated manganese dioxide (1.75 g, 19.9 mmol) was added to a rt (25 °C) solution of *rac*-{4-[(butan-2-yl)amino]-2-(methylthio)pyrimidin-5-yl}methanol (520 mg, 2.29 mmol) in chloroform (50 mL), and the resulting suspension heated to 50 °C for 6 h. After filtration, the mixture was concentrated to a black gum and purified by silica gel chromatography, affording *rac* 4-[(butan-2-yl)amino]-2-(methylthio)pyrimidine-5-carbaldehyde (468 mg, 91%) as a light yellow solid. ¹H NMR (400 MHz, CDCl₃): δ 9.69 (s, 1H), 8.50 (br s, 1H), 8.28 (s, 1H), 4.31 (quin, 1H, J = 7.2 Hz), 2.54 (s, 3H), 1.68–1.61 (m, 2H), 1.26 (d, 3H, J = 6.4 Hz), 0.96 (t, 3H, J = 7.4 Hz); LCMS *m/z*: 225.8 [M + H]⁺.

rac 8-(Butan-2-yl)-2-(methylthio)pyrido[2,3-d]pyrimidin-7(8H)-one. By the method described for the synthesis of 8-cyclopentyl-2-(methylthio)pyrido[2,3-d]pyrimidin-7(8H)-one, *rac* 4-[(butan-2-yl)amino]-2-(methylthio)pyrimidine-5-carbaldehyde (350 mg, 1.5 mmol) was used to produce *rac* 8-(butan-2-yl)-2-(methylthio)pyrido[2,3-d]pyrimidin-7(8H)-one (340 mg, 77%) as a light yellow solid. ¹H NMR (400 MHz, CDCl₃): δ 8.57 (s, 1H), 7.53 (d, 1H, J = 9.6 Hz), 6.59 (br d, 1H, J = 9.6 Hz), 5.58 (br s, 1H), 2.63 (s, 3H), 2.32 (br s, 1H), 1.99 (br s, 1H), 1.61 (br d, 3H, J = 6.4 Hz), 0.83 (t, 3H, J = 7.6 Hz); LCMS *m/z*: 249.8 [M + H]⁺.

(–)-8-(Butan-2-yl)-2-[[1-(methanesulfonyl)piperidin-4-yl]amino]pyrido[2,3-d]pyrimidin-7(8H)-one (**16**) and (+)-8-(Butan-2-yl)-2-[[1-(methanesulfonyl)piperidin-4-yl]amino]pyrido[2,3-d]pyrimidin-7(8H)-one (**16** and **17**). By the same method as **3**, *rac*-8-(butan-2-yl)-2-(methylthio)pyrido[2,3-d]pyrimidin-7(8H)-one was converted in two steps to *rac*-8-(butan-2-yl)-2-[[1-(methanesulfonyl)piperidin-4-yl]amino]pyrido[2,3-d]pyrimidin-7(8H)-one (150 mg, 71% 2-step yield). LCMS *m/z*: 380.0 [M + H]⁺. The enantiomers were resolved by preparative chiral SFC.

The earlier eluting peak afforded 38.56 mg of **16**: LCMS *m/z*: 380.0 [M + H]⁺; ¹H NMR (400 MHz, DMSO-*d*₆, 80 °C): δ 8.55 (s, 1H), 7.64 (d, 1H, J = 9.3 Hz), 7.48 (br d, 1H, J = 6.2 Hz), 6.19 (d, 1H, J = 9.3 Hz), 5.46 (sxt, 1H, J = 7.4 Hz), 4.02–3.89 (m, 1H), 3.61 (ttd, 2H, J = 2.2, 4.2, 12.3 Hz), 2.97–2.89 (m, 2H), 2.88 (s, 3H), 2.27–2.15 (m, 1H), 2.06–1.97 (m, 2H), 1.91 (quind, 1H, J = 7.1, 13.9 Hz), 1.71–1.59 (m, 2H), 1.51 (d, 3H, J = 6.8 Hz), 0.77 (t, 3H, J = 7.5 Hz); ¹³C NMR (DMSO-*d*₆, 151 MHz, 70 °C): δ 162.95, 160.18, 158.70, 155.74, 136.15, 116.24, 104.87, 49.87, 47.01, 43.97, 34.67, 30.40, 25.49, 17.29, 10.78; [α]_D²⁵ –19.5 (c 0.087, CHCl₃); 98.9% ee by chiral analytical SFC/MS [Column: Chiralpak AD-3 150

× 4.6 mm I.D., 3 μm; mobile phase: A: CO₂ B/ethanol (0.05% diethylamine); gradient: from 5 to 40% of B in 5.0 min and hold 40%; for 2.5 min, then 5% of B for 2.5 min; flow rate: 2.5 mL/min; column temperature: 35 °C]; HRMS: calculated for C₁₇H₂₅N₅O₃S [M + H]⁺, 380.1751; found 380.1755.

The later eluting peak afforded 28.92 mg of **17**: LCMS *m/z*: 379.9 [M + H]⁺; ¹H NMR (400 MHz, DMSO-*d*₆, 80 °C): δ 8.54 (s, 1H), 7.64 (d, 1H, J = 9.3 Hz), 7.48 (br d, 1H, J = 6.8 Hz), 6.19 (d, 1H, J = 9.3 Hz), 5.52–5.40 (m, 1H), 4.01–3.89 (m, 1H), 3.61 (ttd, 2H, J = 2.0, 4.1, 12.2 Hz), 2.97–2.89 (m, 2H), 2.88 (s, 3H), 2.27–2.14 (m, 1H), 2.06–1.97 (m, 2H), 1.91 (quind, 1H, J = 7.2, 13.9 Hz), 1.72–1.59 (m, 2H), 1.51 (d, 3H, J = 6.8 Hz), 0.77 (t, 3H, J = 7.5 Hz); ¹³C NMR (101 MHz, DMSO-*d*₆, 80 °C): δ 162.81, 160.12, 158.49, 155.66, 135.92, 116.20, 104.80, 49.83, 46.93, 43.80, 34.80, 30.32/30.29, 25.42, 17.13, 10.60; [α]_D²⁵ +7.56 (c 0.097, CHCl₃); 99.5% ee by chiral analytical SFC/MS. HRMS: calculated for C₁₇H₂₅N₅O₃S [M + H]⁺, 380.1751; found 380.1758. The absolute stereochemistry was not determined for either enantiomer.

2-[[1-(Methanesulfonyl)piperidin-4-yl]amino]-8-(propan-2-yl)pyrido[2,3-d]pyrimidin-7(8H)-one (**18**). By the same method as **3**, 2-(methylthio)-8-(propan-2-yl)pyrido[2,3-d]pyrimidin-7(8H)-one⁴⁷ was converted in two steps to **18** (103.6 mg, 33% 2-step yield) as a solid, after purification by preparative HPLC and lyophilization. LCMS *m/z*: 366.1 [M + H]⁺; ¹H NMR (400 MHz, CDCl₃): δ 8.39 (s, 1H), 7.41 (d, 1H, J = 9.3 Hz), 6.36 (br d, 1H, J = 9.3 Hz), 5.73 (sept, 1H, J = 7.0 Hz), 4.12–3.98 (m, 1H), 3.80 (br d, 2H, J = 11.5 Hz), 2.96 (br t, 2H, J = 11.2 Hz), 2.84 (s, 3H), 2.25–2.16 (m, 2H), 1.78–1.65 (m, 2H), 1.60 (br d, 6H, J = 7.0 Hz); ¹³C NMR (101 MHz, DMSO-*d*₆, 80 °C): δ 162.58, 160.13, 158.46, 155.35, 135.82, 116.33, 104.93, 46.84, 43.88/43.78, 34.76, 30.32, 18.89. HRMS: calculated for C₁₆H₂₃N₅O₃S [M + H]⁺, 366.1594; found 366.1599.

(1R,2R)-2-[[5-(Hydroxymethyl)-2-(methylthio)pyrimidin-4-yl]amino]-1-methylcyclopentan-1-ol. To a solution of (1R,2R)-2-amino-1-methylcyclopentan-1-ol⁵² **25** (21.6 g, 188 mmol) in 2-propanol (~350 mL) was added solid [4-chloro-2-(methylthio)pyrimidin-5-yl]methanol (CAS# 1044145-59-6) (34.8 g, 182 mmol) and DIPEA (95.3 mL, 547 mmol). The mixture was degassed with nitrogen, stirred under a nitrogen atmosphere at rt for 15 min, then at 80 °C for 40 h. The volatiles were removed, and the residual oil (95 g) was partitioned between EtOAc (800 mL) and saturated aqueous NaCl (250 mL). The aqueous layer was further extracted with EtOAc (3 × 500 mL). The combined organic extracts were dried over sodium sulfate, concentrated to oil (75 g), dissolved in EtOAc (200 mL), and heated to 60 °C. Some white solid was observed 5 min after initiation of heating. Heptane (400 mL) was added slowly to the suspension and stirring continued at 60 °C for 15 min. The suspension was cooled to rt and then in an ice–water bath for 15 min. The resulting precipitate was collected by filtration and dried to give (1R,2R)-2-[[5-(hydroxymethyl)-2-(methylthio)pyrimidin-4-yl]amino]-1-methylcyclopentan-1-ol (47.8 g, 97%, 98% ee). LCMS *m/z*: 270.2 [M + H]⁺; ¹H NMR (400 MHz, CDCl₃): δ 7.76 (s, 1H), 6.01 (d, 1H, J = 4.6 Hz), 5.31 (br s, 1H), 4.55 (s, 2H), 4.26 (ddd, 1H, J = 5.7, 8.2, 10.5 Hz), 2.50 (s, 3H), 2.21 (ddd, 1H, J = 3.5, 8.2, 12.1 Hz), 1.97 (dt, 1H, J = 3.5, 7.7 Hz), 1.89–1.76 (m, 2H), 1.75–1.63 (m, 1H), 1.60–1.50 (m, 2H), 1.11 (s, 3H); [α]_D²⁵ +37.7 (c 1.0, MeOH); 98% ee by chiral analytical SFC/MS [Chiralpak IC-3, 4.6 × 150 mm, 3 μm column heated to 25 °C and eluted with a mobile phase of CO₂ and 30% ammonia in methanol (20 mM v/v) flowing at 4.0 mL/min and maintained at 160 bar outlet pressure].

4-[[1(R,2R)-2-Hydroxy-2-methylcyclopentyl]amino]-2-(methylthio)pyrimidine-5-carbaldehyde (**26**). To a 2 L 3-necked flask equipped with a mechanical stirrer and a reflux condenser were added solid manganese dioxide (10 μm mesh, reagent grade, 278 g, 2660 mmol), EtOAc (1.2 L), and solid (1R,2R)-2-[[5-(hydroxymethyl)-2-(methylthio)pyrimidin-4-yl]amino]-1-methylcyclopentan-1-ol (47.7 g, 177 mmol). The flask was heated in a 50 °C oil bath for 4 h. More manganese dioxide (80 g) was added; stirring and heating were continued for another 16 h, until the reaction was completed by LCMS. The solid was removed by filtration, and the flask and filter cake were washed with EtOAc (1 L). The combined filtrates were

filtered again to completely remove trace insolubles and then evaporated to give 4-[[*(1R,2R)*-2-hydroxy-2-methylcyclopentyl]-amino]-2-(methylthio)pyrimidine-5-carbaldehyde **26** (43.8 g, 93%, >98% ee) as a white solid. ¹H NMR (400 MHz, CDCl₃): δ 9.73 (s, 1H), 8.66 (br s, 1H), 8.35 (s, 1H), 4.39 (ddd, 1H, *J* = 6.5, 8.2, 9.6 Hz), 4.16 (s, 1H), 2.57 (s, 3H), 2.33–2.22 (m, 1H), 2.03–1.92 (m, 1H), 1.89–1.68 (m, 3H), 1.68–1.56 (m, 1H), 1.17 (s, 3H); [α]_D²² +12.7 (c 1.0, CHCl₃); >98% ee by chiral analytical SFC/MS [Chiralpak IC-3, 4.6 × 150 mm, 3 μm column heated to 25 °C and eluted with a mobile phase of CO₂ and 30% ammonia in methanol (20 mM v/v) flowing at 4.0 mL/min and maintained at 160 bar outlet pressure]; LCMS *m/z*: 268.2 [M + H]⁺.

8-[[*(1R,2R)*-2-Hydroxy-2-methylcyclopentyl]-2-(methylthio)-pyrido[2,3-*d*]pyrimidin-7(8*H*)-one. To a 2 L three-necked flask equipped with a mechanical stirrer and an internal thermometer were added solid 4-[[*(1R,2R)*-2-hydroxy-2-methylcyclopentyl]amino]-2-(methylthio)pyrimidine-5-carbaldehyde **26** (34.2 g, 128 mmol), THF (400 mL), and EtOAc (33.4 mL, 333 mmol). The solution was purged with nitrogen and cooled in a MeOH–ice bath to –5 °C internal. LiHMDS (1.0 M solution in THF, 4 × 100 mL freshly opened bottles, 400 mmol) was added by cannula, slowly enough to keep the internal temperature at –5 °C. A light yellow precipitate began to form after ~300 mL LiHMDS solution had been added. Stirring was continued as the mixture gradually warmed to rt overnight. The resulting red solution was cooled in an ice–water bath to ~3 °C internal and then EtOH (224 mL, 3840 mmol) was added using a cannula, slowly enough to keep the internal temp at ~3 °C internal. The mixture was stirred in the ice bath for 1 h; then, the cooling bath was removed, the solution was allowed to warm to 20 °C internal and stirring continued for 1 h. The solvents were evaporated, the residue was diluted with water (180 mL) and saturated aqueous NaCl (180 mL), and the aqueous layer was extracted with EtOAc (700 mL, then 2 × 600 mL). The combined organic extracts were dried over sodium sulfate and concentrated to a light yellow-brown foam (43.8 g). This foam was dissolved in EtOAc (70 mL) and sonicated to induce precipitation. The resulting solid was collected by filtration, rinsed with EtOAc (10 mL), and dried to give 8-[[*(1R,2R)*-2-hydroxy-2-methylcyclopentyl]-2-(methylthio)pyrido[2,3-*d*]pyrimidin-7(8*H*)-one (21.4 g, 58%, >99% ee) as a white solid. The mother liquor from the precipitation was evaporated to dryness, the residue (24.5 g) was dissolved in EtOAc (30 mL), and the solution was sonicated to induce precipitation. After filtration and drying, a second crop of the product (4.70 g, 13%, >99% ee) was obtained as a white solid. The total yield for both crops was 26.1 g (71%, >99% ee) after crystallization. ¹H NMR (400 MHz, CDCl₃): δ 8.61 (s, 1H), 7.56 (d, 1H, *J* = 9.4 Hz), 6.60 (d, 1H, *J* = 9.4 Hz), 5.84 (t, 1H, *J* = 8.6 Hz), 2.92–2.76 (m, 1H), 2.64 (s, 3H), 2.34–2.19 (m, 2H), 2.13–2.01 (m, 2H), 2.00–1.81 (m, 2H), 1.16 (s, 3H); [α]_D²² –12.9 (c 1.0, MeOH). >99% ee by analytical chiral SFC/MS [Chiralpak AD-3, 4.6 × 100 mm, 3 μm column heated to 25 °C and eluted with a mobile phase of CO₂ and 40% methanol flowing at 4.0 mL/min and maintained at 120 bar outlet pressure]; LCMS *m/z*: 292.2 [M + H]⁺.

8-[[*(1R,2R)*-2-Hydroxy-2-methylcyclopentyl]-2-[[1-(methanesulfonyl)piperidin-4-yl]amino]pyrido[2,3-*d*]pyrimidin-7(8*H*)-one (**19**). A solution of 8-[[*(1R,2R)*-2-hydroxy-2-methylcyclopentyl]-2-(methylthio)-pyrido[2,3-*d*]pyrimidin-7(8*H*)-one (**27**) (2.33 g, 8.0 mmol), 2-MeTHF (40 mL), water (8 mL), and oxone (12.3 g, 20 mmol) was stirred at rt for 4 h. The solution was cooled in a water bath, diluted with water (10 mL) and saturated aqueous NaCl (10 mL), and extracted with EtOAc (3 × 80 mL). The combined organic extracts were dried over sodium sulfate, evaporated to dark oil (3.76 g), and purified by silica gel chromatography (eluting with a gradient of 20–100% EtOAc in heptane) to give 8-[[*(1R,2R)*-2-hydroxy-2-methylcyclopentyl]-2-(methylsulfonyl)pyrido[2,3-*d*]pyrimidin-7(8*H*)-one (2.2 g, 84%) as a foamy solid. ¹H NMR (400 MHz, CDCl₃): δ 8.96 (s, 1H), 7.74 (d, 1H, *J* = 9.5 Hz), 6.90 (d, 1H, *J* = 9.4 Hz), 5.77 (t, 1H, *J* = 8.5 Hz), 3.40 (s, 3H), 2.92–2.73 (m, 1H), 2.36–2.25 (m, 1H), 2.19–2.08 (m, 2H), 2.03–1.85 (m, 2H), 1.14 (s, 3H); LCMS *m/z*: 306.0 [M-18]⁺. A solution of this sulfone (800 mg, 2.47 mmol) and 1-(methylsulfonyl)piperidin-4-amine (970 mg, 5.44

mmol) in 2-MeTHF (12.4 mL) was heated in a 60 °C oil bath for 24 h. After cooling to rt, the mixture was partitioned between EtOAc (80 mL), water (10 mL), and saturated aqueous NaHCO₃ (10 mL). The aqueous layer was further extracted with EtOAc (2 × 60 mL). The combined organic extracts were dried over sodium sulfate and evaporated to dryness. The residue (1.23 g) was dissolved in EtOAc (11 mL), seed crystals were added, and the solution was allowed to stand at rt overnight. The resulting solid was collected by filtration, rinsed with EtOAc (3 mL), and dried to give 8-[[*(1R,2R)*-2-hydroxy-2-methylcyclopentyl]-2-[[1-(methanesulfonyl)piperidin-4-yl]amino]pyrido[2,3-*d*]pyrimidin-7(8*H*)-one (**19**) (680 mg, 63%, >99% ee) as a white solid. ¹H NMR (400 MHz, CDCl₃): δ 8.43 (s, 1H), 7.45 (d, 1H, *J* = 9.3 Hz), 6.36 (d, 1H, *J* = 9.4 Hz), 5.73 (t, 1H, *J* = 8.4 Hz), 5.34 (br s, 1H), 4.01 (br s, 1H), 3.88–3.74 (m, 2H), 3.01–2.89 (m, 2H), 2.83 (s, 4H), 2.36 (br s, 1H), 2.29–2.14 (m, 3H), 2.03 (dt, 2H, *J* = 2.9, 6.3 Hz), 1.98–1.89 (m, 1H), 1.88–1.81 (m, 1H), 1.78–1.60 (m, 2H), 1.18 (s, 3H); ¹³C NMR (101 MHz, DMSO-*d*₆, 80 °C): δ 162.86, 160.16, 158.50, 156.19, 135.88, 116.59, 104.88, 80.25, 62.96, 47.02, 43.92, 41.53, 34.83, 30.29/30.24, 26.68, 23.49, 22.83; [α]_D²² –17.0 (c 1.0, CHCl₃); >99% ee by chiral analytical SFC/MS [Lux Cellulose-1, 4.6 × 100 mm, 3 μm column heated to 25 °C and eluted with a mobile phase of CO₂ and 5–60% methanol gradient in 3.0 min flowing at 4.0 mL/min and maintained at 120 bar outlet pressure]; HRMS: calculated for C₁₉H₂₇N₅O₄S [M + H]⁺, 422.1857; found 422.1863.

6-Chloro-8-[[*(1R,2R)*-2-hydroxy-2-methylcyclopentyl]-2-[[1-(methanesulfonyl)piperidin-4-yl]amino]pyrido[2,3-*d*]pyrimidin-7(8*H*)-one (**20**). A solution of 8-[[*(1R,2R)*-2-hydroxy-2-methylcyclopentyl]-2-[[1-(methanesulfonyl)piperidin-4-yl]amino]pyrido[2,3-*d*]pyrimidin-7(8*H*)-one (**19**) (4.22 g, 10 mmol) and *N*-chlorosuccinimide (1.53 g, 11 mmol) in 2-MeTHF (100 mL) was stirred in a 50 °C oil bath for 44 h. After cooling to rt, ethanol (1.75 mL, 30 mmol) was added and the mixture stirred at rt for 1 h. The solution was diluted with EtOAc (120 mL) and washed with a mixture of water (15 mL) and saturated aqueous NaHCO₃ (15 mL). The aqueous layer was further extracted with EtOAc (80 mL). The combined organic layers were washed with saturated aqueous NaCl (15 mL), dried over sodium sulfate, filtered, and concentrated to dryness. Ethanol (45 mL) was added to the residue, and the resulting suspension was stirred in a 55 °C oil bath for 1 h, then allowed to cool, while stirring, to rt overnight. The resulting white solid was collected by filtration, rinsed with EtOH (3 mL), and dried under vacuum (~10 mmHg, 50 °C) to give **20** (3.86 g, 84%, >99% ee) as a white solid. ¹H NMR (400 MHz, DMSO-*d*₆, 80 °C): δ 8.60 (s, 1H), 8.02 (s, 1H), 7.61 (br s, 1H), 5.91 (dd, 1H, *J* = 7.4, 9.2 Hz), 4.09 (s, 1H), 4.04–3.94 (m, 1H), 3.70–3.49 (m, 2H), 2.97–2.88 (m, 2H), 2.87 (s, 3H), 2.48–2.42 (m, 1H), 2.20 (dt, 1H, *J* = 8.1, 11.4 Hz), 2.09 (d, 1H, *J* = 12.3 Hz), 2.05–1.96 (m, 2H), 1.96–1.84 (m, 2H), 1.79–1.66 (m, 2H), 1.65–1.51 (m, 1H), 1.01 (s, 3H); ¹³C NMR (101 MHz, DMSO-*d*₆, 80 °C): δ 160.06, 158.58, 158.46, 155.00, 133.82, 119.74, 104.18, 80.25, 64.05, 47.10, 43.88, 41.53, 34.83, 30.21, 30.14, 26.61, 23.42, 22.80; [α]_D²² –31.4 (c 0.4 MeOH); >99% ee by chiral analytical SFC/MS [Phenomenex Lux Cellulose-1 4.6 × 100 mm 3 μm column; rt; mobile phase 30% MeOH in CO₂; 120 bar outlet pressure; flow at 4 mL/min]; HRMS: calculated for C₁₉H₂₆ClN₅O₄S [M + H]⁺, 456.1467; found 456.1472.

(–)-8-[[*(1R*,2R*)*-2-Hydroxy-2-methylcyclopentyl]-6-methyl-2-[[1-(methanesulfonyl)piperidin-4-yl]amino]pyrido[2,3-*d*]pyrimidin-7(8*H*)-one (**21**) and (+)-8-[[*(1R*,2R*)*-2-Hydroxy-2-methylcyclopentyl]-6-methyl-2-[[1-(methanesulfonyl)piperidin-4-yl]amino]pyrido[2,3-*d*]pyrimidin-7(8*H*)-one (**ent-21**). By the same two-step procedure used to make the single-enantiomer analogue 4-[[*(1R,2R)*-2-hydroxy-2-methylcyclopentyl]amino]-2-(methylthio)pyrimidine-5-carbaldehyde (**26**), [4-chloro-2-(methylthio)pyrimidin-5-yl]methanol (92 g, 0.48 mol) and *rac*-(1*R*,2R**)-2-amino-1-methylcyclopentan-1-ol⁵² (72 g, 0.625 mol) were used to prepare 82.6 g of *rac*-4-[[*(1R*,2R*)*-2-hydroxy-2-methylcyclopentyl]amino]-2-(methylthio)pyrimidine-5-carbaldehyde in 64% yield over 2 steps. This aldehyde (6.50 g, 24.3 mmol) was subjected to cyclization with ethyl propionate, sulfur oxidation, and amination using the methods

described in the synthesis of compound 4. This sequence gave 4.48 g of *rac*-8-[(1*R**,2*R**)-2-hydroxy-2-methylcyclopentyl]-2-[[1-(methanesulfonyl)piperidin-4-yl]amino]-6-methylpyrido[2,3-*d*]-pyrimidin-7(8*H*)-one as a white solid in 42% yield over three steps. ¹H NMR (400 MHz, CDCl₃): δ 8.38 (s, 1H), 7.33 (s, 1H), 5.74 (t, 1H, *J* = 8.4 Hz), 5.43–5.21 (m, 1H), 3.97 (br s, 1H), 3.82 (t, 2H, *J* = 10.3 Hz), 2.98–2.87 (m, 2H), 2.83 (s, 3H), 2.47 (br s, 1H), 2.32–2.18 (m, 3H), 2.15 (s, 3H), 2.08–1.57 (m, 3H), 1.16 (s, 3H); LCMS *m/z*: 436.1 [M + H]⁺. To separate the enantiomers, 200 mg of the racemate was submitted to chiral preparative SFC [Chiralpak AD-H 30 × 250 mm column at 36 °C; flow of 40% MeOH in CO₂ held at 100 bar, 80 mL/min; detection with UV 336 nm.]

The earlier eluting peak afforded (+)-8-[(1*R**,2*R**)-2-hydroxy-2-methylcyclopentyl]-2-[[1-(methanesulfonyl)piperidin-4-yl]amino]-6-methylpyrido[2,3-*d*]-pyrimidin-7(8*H*)-one **ent-21** (97.1 mg, >99% ee) as a white solid. ¹H NMR (400 MHz, CDCl₃): δ 8.38 (br s, 1H), 7.33 (s, 1H), 5.75 (t, 1H, *J* = 8.4 Hz), 5.41 (br s, 1H), 4.00 (br s, 1H), 3.81 (t, 2H, *J* = 10.6 Hz), 3.02–2.88 (m, 2H), 2.83 (s, 4H), 2.33–2.18 (m, 3H), 2.16 (s, 3H), 2.09–1.80 (m, 4H), 1.77–1.58 (m, 3H), 1.16 (s, 3H); ¹H NMR (400 MHz, DMSO-*d*₆, 80 °C): δ 8.49 (s, 1H), 7.52 (s, 1H), 7.25 (d, 1H, *J* = 5.5 Hz), 5.87 (t, 1H, *J* = 7.8 Hz), 3.98 (br s, 2H), 3.61 (t, 2H, *J* = 10.8 Hz), 2.97–2.89 (m, 2H, *J* = 6.6 Hz), 2.87 (s, 3H), 2.59–2.52 (m, 1H), 2.33–2.17 (m, 1H), 2.14–2.06 (m, 1H), 2.03 (s, 3H), 2.01–1.82 (m, 4H), 1.76–1.53 (m, 3H), 1.00 (s, 3H); [α]_D²² +31.5 (c 0.1 MeOH); >99% ee by chiral analytical SFC/MS [Chiralpak AD-3 4.6 × 100 mm column; 30% MeOH; 120 bar; 4 mL/min]; LCMS *m/z*: 435.9 [M + H]⁺.

The later eluting peak afforded (–)-8-[(1*R**,2*R**)-2-hydroxy-2-methylcyclopentyl]-2-[[1-(methanesulfonyl)piperidin-4-yl]amino]-6-methylpyrido[2,3-*d*]-pyrimidin-7(8*H*)-one **21** (97.9 mg, ~99% ee) as a white solid. ¹H NMR (400 MHz, CDCl₃): δ 8.39 (br s, 1H), 7.33 (s, 1H), 5.75 (t, 1H, *J* = 8.3 Hz), 5.35 (br s, 1H), 3.99 (br s, 1H), 3.81 (t, 2H, *J* = 10.6 Hz), 3.01–2.88 (m, 2H), 2.83 (s, 4H), 2.33–2.18 (m, 3H), 2.16 (s, 3H), 2.10–1.79 (m, 4H), 1.75–1.53 (m, 3H), 1.16 (s, 3H); ¹H NMR (400 MHz, DMSO-*d*₆, 80 °C): δ 8.49 (br s, 1H), 7.52 (br s, 1H), 7.24 (br s, 1H), 5.87 (t, 1H, *J* = 6.7 Hz), 3.98 (br s, 2H), 3.61 (br s, 2H), 2.91 (br s, 2H), 2.87 (br s, 3H), 2.29–2.17 (m, 1H, *J* = 9.4 Hz), 2.13–2.06 (m, 1H), 2.03 (br s, 3H), 2.00–1.81 (m, 4H), 1.77–1.49 (m, 3H), 1.00 (br s, 3H); ¹³C NMR (101 MHz, DMSO-*d*₆, 80 °C): δ 163.35, 159.66, 157.42, 155.34, 132.19, 124.32, 104.86, 80.27, 63.18, 46.95, 43.93, 41.54, 34.80, 30.33/30.28, 26.75, 23.50, 22.86, 15.94, [α]_D²² –29.8 (c 0.1 MeOH); >99% ee by chiral analytical SFC/MS [Chiralpak AD-3 4.6 × 100 mm column; 30% MeOH; 120 bar; 4 mL/min]; HRMS: calculated for C₂₀H₂₉N₅O₄S [M + H]⁺, 436.2013; found 436.2018. The absolute stereochemistry was not determined for either enantiomer.

6-(Difluoromethyl)-8-[(1*R*,2*R*)-2-hydroxy-2-methylcyclopentyl]-2-[[1-(methanesulfonyl)piperidin-4-yl]amino]pyrido[2,3-*d*]-pyrimidin-7(8*H*)-one (22**).** A 2 L, 4-necked flask equipped with an overhead stirrer, an internal thermometer, and a 250 mL dropping addition funnel was charged with DMSO (1000 mL) and 8-[(1*R*,2*R*)-2-hydroxy-2-methylcyclopentyl]-2-[[1-(methanesulfonyl)piperidin-4-yl]amino]pyrido[2,3-*d*]-pyrimidin-7(8*H*)-one **19** (26.38 g, 64.74 mmol). The mixture was stirred at rt (20 °C) until the solids dissolved completely, then sodium difluoromethanesulfinate (44.7 g, 324 mmol) was added portionwise. Iron(III) chloride on silica gel (105 g of 5 wt % loading, to deliver 5.25 g FeCl₃, 32.4 mmol) was added portionwise, causing a slight exotherm, raising the internal temperature to 25 °C. The dropping addition funnel was charged with a *tert*-butyl hydroperoxide solution (70 wt % in water, 41.7 g, 324 mmol) dissolved in DMSO (100 mL). This solution was added dropwise to the reaction flask at a rate of 1 mL/min, causing the internal temperature to rise to 40 °C by the end of the addition. The mixture was stirred and allowed to cool to rt for 3 h, then poured into saturated aqueous NaCl, and extracted with EtOAc (3 × 100 mL). The combined organic extracts were washed with saturated aqueous NaCl (3 × 100 mL), dried over sodium sulfate, concentrated, and purified by silica gel chromatography (eluting with 20–80% EtOAc in heptane) to give **22** (17.53 g, 57%) as a yellow foam. Two batches of chromatographed **22** (28 g total) were dissolved in acetone,

combined, and concentrated to ~300 mL. MTBE (500 mL) was added and the solution was heated to 50 °C until crystallization occurred. The suspension was sonicated, more MTBE was added (300 mL), and the suspension was allowed to stand at rt for 30 min. Heptane (500 mL total) was added in portions with sonication, then the solids were collected by filtration and washed with heptane. The filtered solids were dissolved in hot ethanol (300 mL). The solution was concentrated under reduced pressure until crystallization began to occur and then allowed to stand at rt for 24 h. Heptane (500 mL) was added, then the solids were collected by filtration and rinsed with additional heptane. The ethanol/heptane filtrate was concentrated to dryness, and the residue was recrystallized in the same manner to afford a second crop. The two crops of precipitate were combined, slurried in hot ethanol (100 mL), sonicated, and allowed to stand at rt for 30 min before heptane (300 mL) was added, and the suspension was allowed to stand at rt for 1.5 h. The resulting crystals were collected by filtration, washed with heptane, and dried to constant volume, affording **22** (18.59 g, 66% for the recrystallization procedure) as a colorless solid. ¹H NMR (400 MHz, DMSO-*d*₆, 80 °C): δ 8.73 (s, 1H), 8.04 (s, 1H), 7.81 (br s, 1H), 6.83 (t, 1H, *J* = 55.3 Hz), 5.87 (dd, 1H, *J* = 7.6, 9.3 Hz), 4.11 (s, 1H), 4.07–3.94 (m, 1H), 3.68–3.56 (m, 2H), 2.97–2.89 (m, 2H), 2.88 (s, 3H), 2.20 (dt, 1H, *J* = 8.8, 11.0 Hz), 2.14–2.05 (m, 1H), 2.05–1.93 (m, 2H), 1.93–1.85 (m, 2H), 1.77–1.66 (m, 2H), 1.66–1.52 (m, 1H), 1.02 (s, 3H). ¹³C NMR (101 MHz, DMSO-*d*₆): δ 161.82–161.61 (m, 1C), 161.55, 161.41, 157.22, 135.42 (t, 1C, *J* = 5.9 Hz), 120.25 (t, 1C, *J* = 20.5 Hz), 112.40 (t, 1C, *J* = 235.5 Hz), 104.48 (br s, 1C), 81.16, 64.24, 48.10, 44.84 (s, 2C), 42.45, 35.73, 31.08 (br d, *J* = 6.4 Hz, 2C), 27.53, 24.38, 23.77. ¹⁹F NMR (376 MHz, DMSO-*d*₆, 80 °C): δ –116.90 (s, 2F). [α]_D²² –22.1 (c 0.5 CHCl₃); *t*_r 2.68 min, >99.5% ee by chiral analytical SFC/MS [Phenomenex Lux Cellulose-1 4.6 × 100 mm 3μ column; rt; mobile phase: 15% MeOH in CO₂; 120 bar; 4 mL/min]; Anal. Calcd for C₂₀H₂₇F₂N₅O₄S: C, 50.95; H, 5.77; N, 14.85; F, 8.06; S, 6.80. Found: C, 51.03; H, 5.78; N, 14.63; F, 7.92; S, 6.75. LCMS *m/z*: 472.2 [M + H]⁺.

Methyl 4,4-Difluorobutanoate. To a solution of 2,2-dimethyl-1,3-dioxane-4,6-dione (Meldrum's acid, 14.4 g, 52 mmol) in CH₂Cl₂ (200 mL) at 0 °C was added difluoroacetic anhydride (17 g, 98 mmol), followed by triethylamine (24.7 g, 245 mmol). The cooling bath was removed and stirring continued at rt for 3 h. The reaction was poured into a separatory funnel, washed with saturated aqueous NaCl (100 mL), dried over sodium sulfate, filtered, and concentrated to dryness. The residue was dissolved in CH₂Cl₂ (200 mL), cooled to 0 °C, washed with 4 M HCl (100 mL) and saturated aqueous NaCl (100 mL), dried over sodium sulfate, filtered, and concentrated to give 5-(2,2-difluoroethyl)-2,2-dimethyl-1,3-dioxane-4,6-dione (11.6 g, 57%, ~90% pure by NMR) as a yellow solid. ¹H NMR (400 MHz, CDCl₃): δ 6.32 (tt, 1H, *J* = 5.0, 57.4 Hz), 3.70 (tt, 1H, *J* = 1.1, 6.2 Hz), 2.62 (ddt, 2H, *J* = 5.1, 6.2, 15.6 Hz), 1.86 (s, 3H), 1.80 (s, 3H); ¹⁹F NMR (377 MHz, CDCl₃): δ –117.59 (s, 2F). Two sealable 350 mL reaction vessels were each charged with 5-(2,2-difluoroethyl)-2,2-dimethyl-1,3-dioxane-4,6-dione (5.3 g, 25 mmol), copper powder (243 mg, 3.82 mmol), pyridine (180 mL), and methanol (20 mL). The suspensions were degassed with nitrogen (3 cycles), sealed, and heated to 120 °C for 4 h. The contents of the two vessels were combined, cooled in an ice/water bath, diluted with CH₂Cl₂ (200 mL), and acidified to pH 2 with 6 M HCl. The organic layer was separated, dried over sodium sulfate, filtered, concentrated, and purified by silica gel chromatography (eluting with CH₂Cl₂) to give methyl 4,4-difluorobutanoate (5.4 g, 70%) as yellow oil. ¹H NMR (400 MHz, CDCl₃): δ 5.93 (tt, 1H, *J* = 4.3, 56.7 Hz), 3.71 (s, 3H), 2.52 (t, 2H, *J* = 7.5 Hz), 2.17 (dt,

2H, $J = 4.3, 7.4, 17.3$ Hz); ^{19}F NMR (376 MHz, CDCl_3): $\delta -117.73$ (s, 2F); ^{13}C NMR (101 MHz, CDCl_3): $\delta 172.43, 116.02$ (t, $J = 238.8$ Hz), 51.91, 29.29 (t, $J = 22.0$ Hz), 26.55 (t, $J = 6.2$ Hz).

6-(2,2-Difluoroethyl)-8-[(1R,2R)-2-hydroxy-2-methylcyclopentyl]-2-(methylthio)pyrido[2,3-*d*]pyrimidin-7(8H)-one. Condensation and cyclization were achieved by using a similar method to the one used in the synthesis of 8-[(1R,2R)-2-hydroxy-2-methylcyclopentyl]-2-(methylthio)pyrido[2,3-*d*]pyrimidin-7(8H)-one but using methyl 4,4-difluorobutanoate (1.34 g, 9.73 mmol) instead of EtOAc and using 4-[(1R,2R)-2-hydroxy-2-methylcyclopentyl]amino-2-(methylthio)pyrimidine-5-carbaldehyde (**26**) (1.00 g, 3.74 mmol). This yielded, after purification by silica gel chromatography, 6-(2,2-difluoroethyl)-8-[(1R,2R)-2-hydroxy-2-methylcyclopentyl]-2-(methylthio)pyrido[2,3-*d*]pyrimidin-7(8H)-one (589 mg, 44%, 70% purity by NMR) as a bright yellow solid, contaminated with a small amount of what appeared to be a vinyl fluoride/H-F elimination side product. ^1H NMR (400 MHz, CDCl_3): $\delta 8.63$ (s, 1H), 7.59 (s, 1H), 6.13 (tt, 1H, $J = 4.6, 57.0$ Hz), 5.88 (t, 1H, $J = 8.6$ Hz), 3.15 (dt, 2H, $J = 4.5, 16.3$ Hz), 2.87–2.72 (m, 1H), 2.64 (s, 3H), 2.32–2.21 (m, 2H), 2.12–2.06 (m, 1H), 2.04–2.01 (m, 1H), 2.00–1.91 (m, 1H), 1.91–1.82 (m, 1H), 1.14 (s, 3H).

6-(2-Fluoropropyl)-8-[(1R,2R)-2-hydroxy-2-methylcyclopentyl]-2-((1-(methylsulfonyl)piperidin-4-yl)amino)pyrido[2,3-*d*]pyrimidin-7(8H)-one (**23**). By the method of **19**, the oxidation of 6-(2,2-difluoroethyl)-8-[(1R,2R)-2-hydroxy-2-methylcyclopentyl]-2-(methylthio)pyrido[2,3-*d*]pyrimidin-7(8H)-one (70% pure, 580 mg, 1.1 mmol), followed by the displacement of the resulting sulfone by 1-(methylsulfonyl)piperidin-4-amine, afforded **23** (389 mg, 70%) as a crystalline solid after recrystallization from EtOAc. ^1H NMR (400 MHz, $\text{DMSO}-d_6$, 80 °C): $\delta 8.58$ (s, 1H), 7.70 (s, 1H), 7.48 (d, 1H, $J = 8.4$ Hz), 6.19 (tt, 1H, $J = 4.6, 57.2$ Hz), 5.89 (dd, 1H, $J = 7.5, 9.4$ Hz), 4.09–4.03 (m, 1H), 4.02–3.91 (m, 1H), 3.68–3.53 (m, 2H), 3.11–3.04 (m, 2H), 3.00 (d, 1H, $J = 4.6$ Hz), 2.96–2.88 (m, 2H), 2.87 (s, 3H), 2.22 (dt, 1H, $J = 8.6, 11.2$ Hz), 2.10 (d, 1H, $J = 10.8$ Hz), 2.04–1.99 (m, 1H), 1.96 (d, 1H, $J = 4.2$ Hz), 1.93–1.80 (m, 2H), 1.77–1.46 (m, 3H), 1.00 (s, 3H); ^{13}C NMR (101 MHz, $\text{DMSO}-d_6$, 80 °C): $\delta 162.87, 160.04, 158.44, 155.61, 135.39, 119.36$ (t, $J = 5.9$ Hz, 1C), 115.42 (t, $J = 239.2$ Hz, 1C), 104.57, 80.27, 63.35, 47.06, 43.92, 41.55, 34.89, 34.59 (t, $J = 24.9$ Hz, 1C), 30.27/30.22, 26.68, 23.45, 22.86; ^{19}F NMR (376 MHz, $\text{DMSO}-d_6$, 80 °C): $\delta -114.46$ (s, 2F); $[\alpha]_D^{25} -25.1$ (c 0.6 MeOH); >99% ee by chiral analytical SFC/MS; HRMS: calcd for $\text{C}_{21}\text{H}_{29}\text{F}_2\text{N}_5\text{O}_4\text{S}$ $[\text{M} + \text{H}]^+$, 486.1981; found 486.1985.

Purification of Cell Cycle Proteins. Purified CDK/cyclin protein complexes were made in-house for CDK1/2/4/6/9 proteins, which were found to be highly active by active site titrations. The details of this work have been previously published.²² Active recombinant human GSK3 β (H350L) expressed by baculovirus in Sf21 insect cells was purchased from Millipore Sigma.

Biochemical Potency Determination by a Mobility Shift Assays. Compounds were tested toward untagged CDK/cyclin kinase complexes produced in-house with a mobility shift assay (MSA) that combines the basic principles of capillary electrophoresis in a microfluidic environment and was performed on a Caliper LabChip EZ Reader II (Caliper Life Science, Hopkinton, MA).⁵³ For example, CDK6/cyclin D1 reactions monitor the phosphorylation of 3 μM 5-carboxyfluorescein (5-FAM)-peptide 34, “Dyrktide” (5-FAM-RRRFRPASPLRGPPK). Inhibitor K_i reactions (45 min) are initiated with 2 mM ATP after a pre-incubation (12 min, 22 °C). Inhibition constant (K_i) values are derived from a fit to the Morrison equation.^{54,55} CDK1/2/4/9 was tested similarly. A detailed method has been previously published.²² Compounds were also tested toward GSK3 β (H350L) with a MSA. GSK3 β (H350L) reactions monitor the phosphorylation of 2 μM 5-FAM-Peptide 15 (5-FAM-KRRELSRRPpSYR-COOH). Inhibitor K_i reactions (30 min) are initiated with 40 μM ATP after a pre-incubation (15 min, 22 °C).

Cell Culture. OVCAR3 cells were obtained from the American Type Culture Collection (ATCC) and maintained in the Roswell Park Memorial Institute (RPMI) 1640 media supplemented with 10%

fetal bovine serum and penicillin–streptomycin. All cells were maintained in a humidified incubator at 37 °C with 5% CO_2 .

Phospho-Serine 807/811 RB1 ELISA. OVCAR3 cells were seeded in growth media and allowed to adhere at 37 °C with 5% CO_2 overnight. OVCAR3 cells were treated overnight with 1 mM hydroxyurea (Sigma-Aldrich) to enrich for G1/S phase cells. OVCAR3 cells were treated with the test compound for 1 h at 37 °C with 5% CO_2 . Cells were lysed, transferred to pre-coated and blocked anti-phospho-Ser807/811 RB1 (Cell Signaling Technology, 8516) ELISA plates for overnight incubation. Plates were washed and total RB1 detection (Cell Signaling Technology, 9309) antibody added. HRP-tagged detection antibody (Cell Signaling Technology, 7076) and Glo substrate reagent (R&D Systems, DY993) was added and incubated. Plates were read in luminescence mode and IC_{50} values calculated using GraphPad Prism v7.02 or Activity Base v8.4.0.154 software by concentration–response nonlinear regression curve fitting utilizing a four-parameter analytical method.

CyQuant Anti-proliferation Assay. OVCAR3 cells were seeded in growth media in 96-well cell culture plates and allowed to adhere at 37 °C with 5% CO_2 overnight. The following day, cells were treated with test compounds for 6 days at 37 °C with 5% CO_2 . CyQUANT Direct nucleic acid stain (Invitrogen, C35011) was performed following the manufacturer’s recommendations to determine the relative viable cell numbers on the Perkin Elmer Envision 2104 Multi Label Reader with a FITC filter in bottom setting. 508/527 nM values were exported and used for IC_{50} calculation using GraphPad Prism v7.02 or Activity Base v8.4.0.154 software by concentration–response nonlinear regression curve fitting utilizing a four-parameter analytical method.

Protein Structure Preparation and MD Simulations. A homology model of the human CDK9 structure and a complex with cyclinT1 were constructed using Prime module in Schrödinger suite 2016–1. The reference coordinates for the complex were obtained from the Protein Data Bank: 4BCH, 3TN8. The modeled complex was used for ligand docking to identify favorable interactions between the ligand molecules and receptor protein. The docking simulation was performed using Glide in Schrödinger, and selected ligand poses were used for MD simulations. A co-crystal structure of CDK2/cyclinE with compound **19** (data not shown) was prepared using Protein preparation wizard in Maestro and used for simulations.

MD simulations were performed using the Desmond module in Schrödinger. Each protein–ligand complex was solvated in a box of TIP3P water molecules using an orthorhombic box under periodic boundary conditions. The overall charge of each system was neutralized by adding Na^+ or Cl^- ions.

The default system relaxation was performed before each simulation, and the temperature and pressure were kept constant at 300 K and 1 bar throughout the simulations. The Simulation Interaction Diagram tool in Schrödinger was used to analyze the detailed interactions between the ligand and protein and root-mean-square deviations (rmsd).

Animal Studies. All animal studies and handling were performed in accordance with Pfizer’s Institutional Animal Care and Use Committee guidelines.

Single Dose Intravenous (IV) and Oral (PO) 22 (PF-06873600) PK in Mice. Municipal water further purified by reverse osmosis and rodent diet were provided ad libitum in this single dose-fed mouse study. PF-06873600 was prepared in 10% *N*-methyl-2-pyrrolidone (NMP)/40% polyethylene glycol 300 (PEG 300)/50% 10 mM citrate buffer to yield concentrations of 0.6 and 1.0 mg/mL for the IV and PO formulations, respectively. $N = 3$ mice each were dosed at 3 mg/kg *via* tail vein (IV) and at 10 mg/kg *via* oral gavage (PO). Approximately, 0.05 mL of blood was collected *via* retro-orbital bleeds in tubes containing K3 EDTA at 0.083, 0.25, 0.5, 1, 3, 7 and, 24 h post-IV dose and 0.25, 0.5, 1, 2, 4, 7, and 24 h post PO dose. Plasma samples were obtained *via* centrifugation and sample cleanup was conducted by protein precipitation with acetonitrile that contained terfenadine as the internal standard (IS). LCMS/MS (AB Sciex QTrap 5500 and Acquity UPLC, USA) quantitation of PF-06873600 and IS was achieved with positive ion MRM transitions of

472.2/354.1 and 472.1/436, respectively. The reversed-phase chromatographic system consisted of a gradient mobile phase at a flow rate of 0.6 mL/min, containing 0.1% formic acid in water and acetonitrile and a Waters HSS T3 1.8 μM 2.1 \times 50 mm column. Analyst version 1.6.2 was used to measure peak areas and peak area ratios of PF-06873600 to IS. A calibration curve was constructed from the peak area ratios (PF-06873600 to IS) with a weighted ($1/x^2$) linear regression using Watson version 7.5 LIMS and a calibration curve ranging between 0.5 and 1000 ng/mL. The PK parameters were determined from individual animal data using noncompartmental analysis in Watson LIMS version 7.5.

Single Dose Intravenous (IV) and Oral (PO) (22) PF-06873600 PK in Dogs. PF-06873600 was prepared in 10% NMP/40% PEG 300/50% 10 mM citrate buffer to yield a concentration of 0.5 mg/mL for the intravenous formulation and in 0.5% methylcellulose containing 0.1% Tween 80 at a concentration of 0.5 mg/mL for the PO formulation. $N = 2$ dogs each were dosed at 0.25 mg/kg *via* cephalic vein (IV) and at 0.5 mg/kg *via* oral gavage (PO). Approximately, 2 mL of blood was collected *via* jugular vein bleeds in tubes containing K3 EDTA at 0.083, 0.25, 0.5, 1, 2, 4, 7, and 24 h post-IV dose and 0.25, 0.5, 1, 2, 4, 7, and 24 h post-PO dose. Plasma samples were obtained *via* centrifugation and sample cleanup was conducted by protein precipitation with acetonitrile that contained propranolol as the IS. LCMS/MS (AB Sciex 6500 and Acquity UPLC, USA) quantitation of PF-06873600 and IS was achieved with positive ion MRM transitions of 472.2/374.1 and 260.2/116.2, respectively. The reversed-phase chromatographic system consisted of a gradient mobile phase at a flow rate of 0.6 mL/min containing 0.1% formic acid in water and acetonitrile and a Waters HSS T3 1.8 μM 2.1 \times 50 mm column. Analyst version 1.5.2 was used to measure peak areas and peak area ratios of PF-06873600 to IS. A calibration curve was constructed from the peak area ratios (PF-06873600 to IS) with a weighted ($1/x^2$) linear regression using Watson version 7.5 LIMS and a calibration curve ranging between 0.5 and 1000 ng/mL. The PK parameters were determined from individual animal data using noncompartmental analysis in Watson LIMS version 7.5.

Tumor Growth Inhibition Studies. Athymic immunocompromised female mice between 6 and 8 weeks of age were implanted with tumor cells from the various Champions TumorGraft models. After the tumors reached 1000–1500 mm³, they were harvested and the tumor fragments were implanted SC in the left flank of the female study mice. Each animal was implanted with a passage lot 7 for CTG-0192, CTG-0464 tumor growth was monitored twice a week using digital calipers and the tumor volume (TV) was calculated using the formula ($0.52 \times [\text{length} \times \text{width}^2]$). When the TV reached an average volume of 150–300 mm³, animals were matched by the tumor size and assigned into the vehicle control and PF-06873600 30 mg/kg groups ($n = 5$) and dosing was initiated on day 0 using a BID schedule for vehicle control and PF-06873600. After the initiation of dosing on day 0, animals were weighed twice per week using a digital scale and TV was measured twice per week and also on the final day of study or on the day moribund animals were euthanized. The study was terminated when the mean tumor volume of the vehicle control group reached 1500 mm³ or day 60, whichever happened sooner.

Single-Crystal X-ray Structure of 22 at 100 K. The single-crystal X-ray diffraction studies were carried out on a Bruker Kappa APEX-II CCD diffractometer equipped with Cu K α radiation ($\lambda = 1.5478$). Crystals of the subject compound were grown by dissolving approximately 1 mg of the sample in 350 μL of dichloroethane, which was then vapor diffused with pentane over 2 days. A $0.251 \times 0.079 \times 0.064$ mm piece of a colorless block was mounted on a cryoloop with paratone oil. Data were collected in a nitrogen gas stream at 100(2) K using ϕ and ω scans. Crystal-to-detector distance was 40 mm using variable exposure time (2s–5s), depending on θ with a scan width of 2.0°. Data collection was 99.5% complete to 68.00° in θ . A total of 37376 reflections were collected covering the indices, $-29 \leq h \leq 30$, $-7 \leq k \leq 7$, $-30 \leq l \leq 28$. 7702 reflections were found to be symmetry independent, with a R_{int} of 0.0601. Indexing and unit cell refinement indicated a C-centered, monoclinic lattice. The space group was found to be C2. The data were integrated using the Bruker

SAINT software program and scaled using the SADABS software program. Solution by direct methods (SHELXT) produced a complete phasing model consistent with the proposed structure.

All nonhydrogen atoms were refined anisotropically by full-matrix least-squares (SHELXL-2014). All hydrogen atoms were placed using a riding model. Their positions were constrained relative to their parent atom using the appropriate HFIX command in SHELXL-2014. The absolute stereochemistry of the molecule was established by anomalous dispersion using the Parson's method with a Flack parameter of 0.022(12). Crystallographic data are summarized in the Supporting Information.

CDK2/CyclinE1 Protein Production and Crystallography. The cDNAs encoding human full-length CDK2 and residues 96–378 of human cyclin E1 with an N-terminal His tag were synthesized and cloned into pFastBack1 and pKRIC-N6, respectively, and then expressed separately in insect cells. Cells were mixed, lysed in lysis buffer (40 mM HEPES, pH 7.5, 150 mM NaCl, 0.01% 1-thioglycerol, and 25 mM imidazole), and lysates were cleared by centrifugation. The complex was purified on a Probond column with lysis buffer wash, followed by step elution at 250 mM imidazole. His tags were cleaved from cyclinE1 with TEV and dialyzed overnight. The proteins flowed over a Probond column again. The complexes were phosphorylated by CDK7/cyclinH1/Mat1 in a final buffer supplemented with 5 mM ATP and 10 mM MgCl₂ and incubated for 1 h at room temperature. The proteins flowed over a Probond column to remove the His-tagged CDK7 complex; the complex was then loaded on a Superdex 200 in a final buffer of 40 mM HEPES, pH7.5, 150 mM NaCl, 0.01% 1-thioglycerol. The phosphorylated CDK2/cyclinE1 complex at a concentration of 13.25 mg/mL (combined) was filtered with a low-protein binding 0.45 μM membrane and set up for crystallization in MRC 48-well plates. Sitting drops in a 1:1 ratio (protein/well solution) with a well solution containing 0.1 M MES at pH 6, 0.18 M magnesium formate, and 9.0% (w/v) PEG 20000 were incubated at 21 °C for 24 h. After one day, drops were streak-seeded using a probe that was dipped into a "seed stock" solution (a previously grown CDK2/cyclinE1 crystal crushed into 1 mL of well solution). Data quality crystals grew 5–7 days after seeding. Apo crystals were then introduced to 1 mM (final concentration) of the inhibitor compound (2, 4, or 22) in 100% DMSO, *in situ*. After a 2 h soak, the crystals were then placed into a cryoprotectant-containing well solution + 22% glycerol before they were flash-frozen in liquid N₂. X-ray diffraction data were collected at the Advanced Photon Source beamline 17-ID and processed with autoPROC from Global Phasing.⁵⁶ Structure solution and refinement were done using BUSTER⁵⁷ and COOT.⁵⁸ The final refined 2.4 Å resolution structure with 22 has been deposited to the Protein Data Bank (www.pdb.org) with ID code 7KJS.

■ ASSOCIATED CONTENT

Supporting Information

The Supporting Information is available free of charge at <https://pubs.acs.org/doi/10.1021/acs.jmedchem.1c00159>.

Molecular formula strings (CSV)

CDK2/cyclinE1/inhibitor complex crystal structure statistics for 22, single-crystal X-ray structure data for 22, *in vitro* biochemical activity of 22, kinase inhibition panel data for 22, ¹H and ¹³C NMR spectra of compounds 8 and 22, and ¹⁹F NMR spectrum of 22 (PDF)

■ AUTHOR INFORMATION

Corresponding Author

Kevin D. Freeman-Cook – Pfizer Global Research and Development La Jolla, San Diego, California 92121, United States; orcid.org/0000-0001-9014-2309; Email: kevin.freeman-cook@pfizer.com

Authors

Robert L. Hoffman – Pfizer Global Research and Development La Jolla, San Diego, California 92121, United States; orcid.org/0000-0002-2030-9094

Douglas C. Behenna – Pfizer Global Research and Development La Jolla, San Diego, California 92121, United States

Britton Boras – Pfizer Global Research and Development La Jolla, San Diego, California 92121, United States

Jordan Carelli – Pfizer Global Research and Development La Jolla, San Diego, California 92121, United States

Wade Diehl – Pfizer Global Research and Development La Jolla, San Diego, California 92121, United States

Rose Ann Ferre – Pfizer Global Research and Development La Jolla, San Diego, California 92121, United States

You-Ai He – Pfizer Global Research and Development La Jolla, San Diego, California 92121, United States

Andrea Hui – Pfizer Global Research and Development La Jolla, San Diego, California 92121, United States

Buwen Huang – Pfizer Global Research and Development La Jolla, San Diego, California 92121, United States

Nanni Huser – Pfizer Global Research and Development La Jolla, San Diego, California 92121, United States

Rhys Jones – Pfizer Global Research and Development La Jolla, San Diego, California 92121, United States

Susan E. Kephart – Pfizer Global Research and Development La Jolla, San Diego, California 92121, United States

John Lapek – Pfizer Global Research and Development La Jolla, San Diego, California 92121, United States;

orcid.org/0000-0002-6578-5350

Michele McTigue – Pfizer Global Research and Development La Jolla, San Diego, California 92121, United States

Nichol Miller – Pfizer Global Research and Development La Jolla, San Diego, California 92121, United States

Brion W. Murray – Pfizer Global Research and Development La Jolla, San Diego, California 92121, United States

Asako Nagata – Pfizer Global Research and Development La Jolla, San Diego, California 92121, United States

Lisa Nguyen – Pfizer Global Research and Development La Jolla, San Diego, California 92121, United States

Sherry Niessen – Pfizer Global Research and Development La Jolla, San Diego, California 92121, United States

Sacha Ninkovic – Pfizer Global Research and Development La Jolla, San Diego, California 92121, United States

Inish O'Doherty – Pfizer Global Research and Development La Jolla, San Diego, California 92121, United States

Martha A. Ornelas – Pfizer Global Research and Development La Jolla, San Diego, California 92121, United States

James Solowiej – Pfizer Global Research and Development La Jolla, San Diego, California 92121, United States

Scott C. Sutton – Pfizer Global Research and Development La Jolla, San Diego, California 92121, United States

Khanh Tran – Pfizer Global Research and Development La Jolla, San Diego, California 92121, United States

Elaine Tseng – Pfizer Global Research and Development, Groton, Connecticut 06340, United States

Ravi Visswanathan – Pfizer Global Research and Development La Jolla, San Diego, California 92121, United States

Meirong Xu – Pfizer Global Research and Development La Jolla, San Diego, California 92121, United States

Luke Zehnder – Pfizer Global Research and Development La Jolla, San Diego, California 92121, United States

Qin Zhang – Pfizer Global Research and Development La Jolla, San Diego, California 92121, United States

Cathy Zhang – Pfizer Global Research and Development La Jolla, San Diego, California 92121, United States

Stephen Dann – Pfizer Global Research and Development La Jolla, San Diego, California 92121, United States

Complete contact information is available at:

<https://pubs.acs.org/10.1021/acs.jmedchem.1c00159>

Notes

The authors declare no competing financial interest.

ACKNOWLEDGMENTS

The authors would like to thank the Pfizer La Jolla Discovery Technology group who were responsible for all HRMS, preparative HPLC, and SFC separations. The authors would also like to thank Alex Yanovsky and the UCSD X-ray facility for small-molecule X-ray crystal structure determination. We also thank Martin Edwards for extraordinary mentorship, advice, and editing of the manuscript.

ABBREVIATIONS

AcOH, acetic acid; ADME, absorption, distribution, metabolism, and excretion; APCI, atmospheric-pressure chemical ionization; br s, broad singlet; CDK, cyclin-dependent kinase; DIPEA, diisopropylethylamine; d, doublet; dd, doublet of doublets; DMF, *N,N*-dimethylformamide; DMSO, dimethyl sulfoxide; dt, doublet of triplets; ESI, electrospray ionization; ee, enantiomeric excess; ER+, estrogen receptor positive; EtOAc, ethyl acetate; GI, gastrointestinal; HPLC, high-performance liquid chromatography; h, hour(s); HLM, human liver microsomes; LCMS, liquid chromatography–mass spectrometry; LipE, lipophilic efficiency; LiHMDS, lithium hexamethyldisilazide; LOO, leave-one-out; MDCK-LE, Madin–Darby canine kidney low efflux cell line; MD, molecular dynamics; MMP, matched molecular pair; MSA, mobility shift assay; MTBE, methyl *tert*-butyl ether; min, minute(s); NSCLC, non-small cell lung cancer; ppm, part per million; q, quartet; quint, quintet; RB1, retinoblastoma protein; rmsd, root-mean-squared deviation of atomic distance; RRCK, Ralph Russ canine kidney cell based; rt, room temperature; s, singlet; sept, septet; SFC, supercritical fluid chromatography; t, triplet; THF, tetrahydrofuran; TIC, total ion chromatogram; TLC, thin-layer chromatography

REFERENCES

- (1) Lim, S.; Kaldis, P. Cdks, cyclins; CKIs roles beyond cell cycle regulation. *Development* **2013**, *140*, 3079–3093.
- (2) Malumbres, M. Cyclin-dependent kinases. *Genome Biol.* **2014**, *15*, 122.
- (3) Schwartz, G. K.; Shah, M. A. Targeting the cell cycle: a new approach to cancer therapy. *J. Clin. Oncol.* **2005**, *23*, 9408–9421.
- (4) Hunter, T.; Pines, J. Cyclins and cancer II: cyclin D and CDK inhibitors come of age. *Cell* **1994**, *79*, 573–582.
- (5) Malumbres, M.; Barbacid, M. Milestones in cell division: to cycle or not to cycle: a critical decision in cancer. *Nat. Rev. Cancer* **2001**, *1*, 222–231.
- (6) Hanahan, D.; Weinberg, R. A. Hallmarks of cancer: the next generation. *Cell* **2011**, *144*, 646–674.
- (7) Malumbres, M.; Barbacid, M. Cell cycle, CDKs and cancer: a changing paradigm. *Nat. Rev. Cancer* **2009**, *9*, 153–166.
- (8) Musgrove, E. A.; Caldon, C. E.; Barraclough, J.; Stone, A.; Sutherland, R. L. Cyclin D as a therapeutic target in cancer. *Nat. Rev. Cancer* **2011**, *11*, 558–572.

- (9) VanArsdale, T.; Boshoff, C.; Arndt, K. T.; Abraham, R. T. Molecular Pathways: Targeting the cyclin D-CDK4/6 axis for cancer treatment. *Clin. Cancer Res.* **2015**, *21*, 2905–2910.
- (10) Hu, S.; Lu, Y.; Orr, B.; Godek, K.; Mustachio, L. M.; Kawakami, M.; Sekula, D.; Compton, D. A.; Freemantle, S.; Dmitrovsky, E. Specific CP110 phosphorylation sites mediate anaphase catastrophe after CDK2 inhibition: evidence for cooperation with USP33 knockdown. *Mol. Cancer Ther.* **2015**, *14*, 2576–2585.
- (11) Molenaar, J. J.; Ebus, M. E.; Geerts, D.; Koster, J.; Lamers, F.; Valentijn, L. J.; Westerhout, E. M.; Versteeg, R.; Caron, H. N. Inactivation of CDK2 is synthetically lethal to MYCN over-expressing cancer cells. *Proc. Natl. Acad. Sci. U.S.A.* **2009**, *106*, 12968–12973.
- (12) Du, J.; Widlund, H. R.; Horstmann, M. A.; Ramaswamy, S.; Ross, K.; Huber, W. E.; Nishimura, E. K.; Golub, T. R.; Fisher, D. E. Critical role of CDK2 for melanoma growth linked to its melanocyte-specific transcriptional regulation by MITF. *Cancer Cell* **2004**, *6*, 565–576.
- (13) Ying, M.; Shao, X.; Jing, H.; Liu, Y.; Qi, X.; Cao, J.; Chen, Y.; Xiang, S.; Song, H.; Hu, R.; Wei, G.; Yang, B.; He, Q. Ubiquitin-dependent degradation of cdk2 drives the therapeutic differentiation of aml by targeting prdx2. *Blood* **2018**, *131*, 2698–2711.
- (14) Li, Y.; Yang, X. H.; Fang, S. J.; Qin, C. F.; Sun, R. L.; Liu, Z. Y.; Jiang, B. Y.; Wu, X.; Li, G. HOXA7 stimulates human hepatocellular carcinoma proliferation through cyclin E1/CDK2. *Oncol. Rep.* **2015**, *33*, 990–996.
- (15) Wang, J.; Yang, T.; Xu, G.; Liu, H.; Ren, C.; Xie, W.; Wang, M. Cyclin-dependent kinase 2 promotes tumor proliferation and induces radio resistance in glioblastoma. *Transl. Oncol.* **2016**, *9*, 548–556.
- (16) Yin, X.; Yu, J.; Zhou, Y.; Wang, C.; Jiao, Z.; Qian, Z.; Sun, H.; Chen, B. Identification of CDK2 as a novel target in treatment of prostate cancer. *Future Oncol.* **2018**, *14*, 709–718.
- (17) Caldon, C. E.; Sergio, C. M.; Kang, J.; Muthukaruppan, A.; Boersma, M. N.; Stone, A.; Barraclough, J.; Lee, C. S.; Black, M. A.; Miller, L. D.; Gee, J. M.; Nicholson, R. I.; Sutherland, R. L.; Print, C. G.; Musgrove, E. A. Cyclin E2 overexpression is associated with endocrine resistance but not insensitivity to CDK2 inhibition in human breast cancer cells. *Mol. Cancer Ther.* **2012**, *11*, 1488–1499.
- (18) Trowbridge, J. M.; Rogatsky, I.; Garabedian, M. J. Regulation of estrogen receptor transcriptional enhancement by the cyclin A/Cdk2 complex. *Proc. Natl. Acad. Sci. U.S.A.* **1997**, *94*, 10132–10137.
- (19) Pierson-Mullany, L. K.; Lange, C. A. Phosphorylation of progesterone receptor serine 400 mediates ligand-independent transcriptional activity in response to activation of cyclin-dependent protein kinase 2. *Mol. Cell. Biol.* **2004**, *24*, 10542–10557.
- (20) Akli, S.; Van Pelt, C. S.; Bui, T.; Meijer, L.; Keyomarsi, K. Cdk2 is required for breast cancer mediated by the low-molecular-weight isoform of cyclin. *E. Cancer Res.* **2011**, *71*, 3377–3386.
- (21) Rosen, D. G.; Yang, G.; Deavers, M. T.; Malpica, A.; Kavanagh, J. J.; Mills, G. B.; Liu, J. Cyclin E expression is correlated with tumor progression and predicts a poor prognosis in patients with ovarian carcinoma. *Cancer* **2006**, *106*, 1925–1932.
- (22) Chen, P.; Lee, N. V.; Hu, W.; Xu, M.; Ferre, R. A.; Lam, H.; Bergqvist, S.; Solowiej, J.; Diehl, W.; He, Y.-A.; Yu, X.; Nagata, A.; VanArsdale, T.; Murray, B. W. Spectrum and degree of CDK drug interactions predicts clinical performance. *Mol. Cancer Ther.* **2016**, *15*, 2273–2281.
- (23) Herrera-Abreu, M. T.; Palafox, M.; Asghar, U.; Rivas, M. A.; Cutts, R. J.; Garcia-Murillas, L.; Pearson, A.; Guzman, M.; Rodriguez, O.; Grueso, J.; Bellet, M.; Cortés, J.; Elliott, R.; Pancholi, S.; Lord, C. J.; Baselga, J.; Dowsett, M.; Martin, L.-A.; Turner, N. C.; Serra, V. Early adaptation and acquired resistance to CDK4/6 inhibition in estrogen receptor-positive breast cancer. *Cancer Res.* **2016**, *76*, 2301–2313.
- (24) Kuhn, E.; Bahadirli-Talbot, A.; Shih, I.-M. Frequent CCNE1 amplification in endometrial intraepithelial carcinoma and uterine serous carcinoma. *Mod. Pathol.* **2014**, *27*, 1014–1019.
- (25) Turner, N. C.; Liu, Y.; Zhu, Z.; Loi, S.; Colleoni, M.; Loibl, S.; Demechele, A.; Harbeck, N.; André, F.; Bayar, M. A.; Michiels, S.; Zhang, Z.; Giorgetti, C.; Arnedos, M.; Huang Bartlett, C.; Cristofanilli, M. Cyclin E1 expression and palbociclib efficacy in previously treated hormone receptor-positive metastatic breast cancer. *J. Clin. Oncol.* **2019**, *37*, 1169–1178.
- (26) Patel, V.; Senderowicz, A. M.; Pinto, D., Jr.; Igishi, T.; Raffeld, M.; Quintanilla-Martinez, L.; Ensley, J. F.; Sausville, E. A.; Gutkind, J. S. Flavopiridol, a novel cyclin-dependent kinase inhibitor, suppresses the growth of head and neck squamous cell carcinomas by inducing apoptosis. *J. Clin. Invest.* **1998**, *102*, 1674–1681.
- (27) Senderowicz, A. M. Flavopiridol: the first cyclin-dependent kinase inhibitor in human clinical trials. *Invest. New Drugs* **1999**, *17*, 313–320.
- (28) Jorda, R.; Hendrychová, D.; Voller, J.; Řezníčková, E.; Gucký, T.; Kryštof, V. How selective are pharmacological inhibitors of cell-cycle-regulating cyclin-dependent kinases? *J. Med. Chem.* **2018**, *61*, 9105–9120.
- (29) Burdette-Radoux, S.; Tozer, R. G.; Lohmann, R. C.; Quirt, I.; Ernst, D. S.; Walsh, W.; Wainman, N.; Colevas, A. D.; Eisenhauer, E. A. Phase II trial of flavopiridol, a cyclin dependent kinase inhibitor, in untreated metastatic malignant melanoma. *Invest. New Drugs* **2004**, *22*, 315–322.
- (30) Jessen, B. A.; Lee, L.; Koudriakova, T.; Haines, M.; Lundgren, K.; Price, S.; Nonomiya, J.; Lewis, C.; Stevens, G. J. Peripheral white blood cell toxicity induced by broad spectrum cyclin-dependent kinase inhibitors. *J. Appl. Toxicol.* **2007**, *27*, 133–142.
- (31) Santamaría, D.; Barrière, C.; Cerqueira, A.; Hunt, S.; Tardy, C.; Newton, K.; Cáceres, J. F.; Dubus, P.; Malumbres, M.; Barbacid, M. Cdk1 is sufficient to drive the mammalian cell cycle. *Nature* **2007**, *448*, 811–815.
- (32) Kramer, C.; Heinisch, T.; Fligge, T.; Beck, B.; Clark, T. A consistent dataset of kinetic solubilities for early-phase drug discovery. *ChemMedChem* **2009**, *4*, 1529–1536.
- (33) Waring, M. J. Defining optimum lipophilicity and molecular weight ranges for drug candidates-molecular weight dependent lower log D limits based on permeability. *Bioorg. Med. Chem. Lett.* **2009**, *19*, 2844–2851.
- (34) Johnson, T. W.; Dress, K. R.; Edwards, M. Using the golden triangle to optimize clearance and oral absorption. *Bioorg. Med. Chem. Lett.* **2009**, *19*, 5560–5564.
- (35) Peters, J.-U.; Schneider, P.; Mattei, P.; Kansy, M. Pharmacological promiscuity: dependence on compound properties and target specificity in a set of recent roche compounds. *ChemMedChem* **2009**, *4*, 680–686.
- (36) Freeman-Cook, K. D.; Hoffman, R. L.; Johnson, T. W. Lipophilic efficiency: the most important efficiency metric in medicinal chemistry. *Future Med. Chem.* **2013**, *5*, 113–115.
- (37) Zhao, Q.; Ouyang, X.; Wan, X.; Gajiwala, K. S.; Kath, J. C.; Jones, L. H.; Burlingame, A. L.; Taunton, J. Broad-spectrum kinase profiling in live cells with lysine-targeted sulfonyl fluoride probes. *J. Am. Chem. Soc.* **2017**, *139*, 680–685.
- (38) Free, S. M., Jr.; Wilson, J. W. A mathematical contribution to structure-activity studies. *J. Med. Chem.* **1964**, *7*, 395–399.
- (39) Freeman-Cook, K. D.; Amor, P.; Bader, S.; Buzon, L. M.; Coffey, S. B.; Corbett, J. W.; Dirico, K. J.; Doran, S. D.; Elliott, R. L.; Esler, W.; Guzman-Perez, A.; Henegar, K. E.; Houser, J. A.; Jones, C. S.; Limberakis, C.; Loomis, K.; McPherson, K.; Murdande, S.; Nelson, K. L.; Phillion, D.; Pierce, B. S.; Song, W.; Sugarman, E.; Tapley, S.; Tu, M.; Zhao, Z. Maximizing lipophilic efficiency: The use of Free-Wilson analysis in the design of inhibitors of acetyl-CoA carboxylase. *J. Med. Chem.* **2012**, *55*, 935–942.
- (40) Freeman-Cook, K.; Hoffman, R. L.; Miller, N.; Nguyen, L.; Wang, T.; Almaden, J.; Chionis, J.; Eisele, K.; Liu, C.; Zhang, Q.; Niessen, S.; Lapek, J.; Weinrich, S. L.; Wei, P.; Carelli, J.; Lee, N.; Zhang, C.; Huser, N.; Looper, D.; Ninkovic, S.; McTigue, M.; Behenna, D.; Ferre, R. A.; He, Y.; Tran, K. T.; Sutton, S.; Zehnder, L. R.; Kephart, S. E.; Nagata, A.; Ornelas, M. A.; Murray, B.; Xu, M.; Solowiej, J. E.; Visswanathan, R.; Boras, B.; Wilson, E.; Oderup, C.; Salek-Ardakani, S.; Zhu, Z.; McMillan, E.; Mu, X. J.; Ding, Y.; Kan, Z.; Bienkowska, J. R.; VanArsdale, T.; White, M. A.; Dann, S. G.

Expanding control of the tumor cell cycle; discovery of the CDK2/4/6 inhibitor PF-06873600 *Cancer Cell*. Unpublished results.

(41) Di, L.; Whitney-Pickett, C.; Umland, J. P.; Zhang, H.; Zhang, X.; Gebhard, D. F.; Lai, Y.; Federico, J. J.; Davidson, R. E.; Smith, R.; Reyner, E. L.; Lee, C.; Feng, B.; Rotter, C.; Varma, M. V.; Kempshall, S.; Fenner, K.; El-kattan, A. F.; Liston, T. E.; Troutman, M. D. Development of a new permeability assay using low-efflux MDCKII cells. *J. Pharm. Sci.* **2011**, *100*, 4974–4985.

(42) Davis, R. J.; Welcker, M.; Clurman, B. E. Tumor suppression by the Fbw7 ubiquitin ligase: mechanisms and opportunities. *Cancer Cell* **2014**, *26*, 455–464.

(43) Takada, M.; Zhang, W.; Suzuki, A.; Kuroda, T. S.; Yu, Z.; Inuzuka, H.; Gao, D.; Wan, L.; Zhuang, M.; Hu, L.; Zhai, B.; Fry, C. J.; Bloom, K.; Li, G.; Karpen, G. H.; Wei, W.; Zhang, Q. FBW7 loss promotes chromosomal instability and tumorigenesis via cyclin E1/CDK2-mediated phosphorylation of CENP-A. *Cancer Res.* **2017**, *77*, 4881–4893.

(44) Bailey, M. H.; Tokheim, C.; Porta-Pardo, E.; Sengupta, S.; Bertrand, D.; Weerasinghe, A.; Colaprico, A.; Wendl, M. C.; Kim, J.; Reardon, B.; Ng, P. K.-S.; Jeong, K. J.; Cao, S.; Wang, Z.; Gao, J.; Gao, Q.; Wang, F.; Liu, E. M.; Mularoni, L.; Rubio-Perez, C.; Nagarajan, N.; Cortes-Ciriano, I.; Zhou, D. C.; Liang, W.-W.; Hess, J. M.; Yellapantula, V. D.; Tamborero, D.; Gonzalez-Perez, A.; Suphavitai, C.; Ko, J. Y.; Khurana, E.; Park, P. J.; Van Allen, E. M.; Liang, H.; Lawrence, M. S.; Godzik, A.; Lopez-Bigas, N.; Stuart, J.; Wheeler, D.; Getz, G.; Chen, K.; Lazar, A. J.; Mills, G. B.; Karchin, R.; Ding, L. Comprehensive characterization of cancer driver genes and mutations. *Cell* **2018**, *173*, 371–385.

(45) Greene, T. W.; Wuts, P. G. M. *Protective Groups in Organic Synthesis*, 2nd ed.; John Wiley and Sons, Inc., 1991.

(46) VanderWel, S. N.; Harvey, P. J.; McNamara, D. J.; Repine, J. T.; Keller, P. R.; Quin, J., III; Booth, R. J.; Elliott, W. L.; Dobrusin, E. M.; Fry, D. W.; Toogood, P. L. Pyrido[2,3-d]pyrimidin-7-ones as specific inhibitors of cyclin-dependent kinase 4. *J. Med. Chem.* **2005**, *48*, 2371–2387.

(47) Barvian, M.; Boschelli, D. H.; Cossrow, J.; Dobrusin, E.; Fattaey, A.; Fritsch, A.; Fry, D.; Harvey, P.; Keller, P.; Garrett, M.; La, F.; Leopold, W.; McNamara, D.; Quin, M.; Trumpp-Kallmeyer, S.; Toogood, P.; Wu, Z.; Zhang, E. Pyrido[2,3-d]pyrimidin-7-one inhibitors of cyclin-dependent kinases. *J. Med. Chem.* **2000**, *43*, 4606–4616.

(48) Toogood, P. L.; Harvey, P. J.; Repine, J. T.; Sheehan, D. J.; VanderWel, S. N.; Zhou, H.; Keller, P. R.; McNamara, D. J.; Sherry, D.; Zhu, T.; Brodfuehrer, J.; Choi, C.; Barvian, M. R.; Fry, D. W. Discovery of a potent and selective inhibitor of cyclin-dependent Kinase 4/6. *J. Med. Chem.* **2005**, *48*, 2388–2406.

(49) Fujiwara, Y.; Dixon, J. A.; Rodriguez, R. A.; Baxter, R. D.; Dixon, D. D.; Collins, M. R.; Blackmond, D. G.; Baran, P. S. A new reagent for direct difluoromethylation. *J. Am. Chem. Soc.* **2012**, *134*, 1494–1497.

(50) O'Hara, F.; Blackmond, D. G.; Baran, P. S. Radical-based regioselective C-H functionalization of electron-deficient heteroarenes: scope, tunability, and predictability. *J. Am. Chem. Soc.* **2013**, *135*, 12122.

(51) Wiehl, W.; Frahm, A. W. Asymmetric reductive amination of cycloalkanones. 5. Synthesis and absolute configuration of 2-substituted cyclopentanamines. *Chem. Ber.* **1986**, *119*, 2668–2677.

(52) Behenna, D. C.; Chen, P.; Freeman-Cook, K. D.; Hoffman, R. L.; Jalaie, M.; Nagata, A.; Nair, S. K.; Ninkovic, S.; Ornelas, M. A.; Palmer, C. L.; Rui, E. Y. Preparation of heterocyclaminopyrido[2,3-d]pyrimidin-7(8H)-one compounds as cyclin-dependent kinase inhibitors for treatment of proliferative diseases such as cancer. U.S. Patent 20,180,044,344 A1, 2018.

(53) Perrin, D.; Frémaux, C.; Shutes, A. Capillary microfluidic electrophoretic mobility shift assays: application to enzymatic assays in drug discovery. *Expert Opin. Drug Discovery* **2010**, *5*, 51–63.

(54) Morrison, J. F. Kinetics of the reversible inhibition of enzyme-catalyzed reactions by tight-binding inhibitors. *Biochim. Biophys. Acta, Enzymol.* **1969**, *185*, 269–286.

(55) Murphy, D. J. Determination of accurate KI values for tight-binding enzyme inhibitors: an in silico study of experimental error and assay design. *Anal. Biochem.* **2004**, *327*, 61–67.

(56) Vonrhein, C.; Flensburg, C.; Keller, P.; Sharff, A.; Smart, O.; Paciorek, W.; Womack, T.; Bricogne, G. Data processing and analysis with the autoPROC toolbox. *Acta Crystallogr., Sect. D: Biol. Crystallogr.* **2011**, *67*, 293–302.

(57) Bricogne, G.; Blanc, E.; Brandl, M.; Flensburg, C.; Keller, P.; Paciorek, W.; Roversi, P.; Sharff, A.; Smart, O.; Vonrhein, C. *BUSTER*; Global Phasing Ltd: Cambridge, United Kingdom, 2011–2020.

(58) Emsley, P.; Cowtan, K. Coot: model-building tools for molecular graphics. *Acta Crystallogr., Sect. D: Biol. Crystallogr.* **2004**, *60*, 2126–2132.